CO-CONSOLIDATION OF ADDITIVELY MANUFACTURED, PATTERNED METAL INTERFACES WITH THERMOPLASTIC COMPOSITES USING AUTOMATED FIBER PLACEMENT

by
ÖZKAN OKAN

Submitted to the Graduate School of Engineering and Natural Sciences
in partial fulfilment of
the requirements for the degree of
Master of Science

Sabancı University
JULY 2022

ABSTRACT

CO-CONSOLIDATION OF ADDITIVELY MANUFACTURED, PATTERNED METAL INTERFACES WITH THERMOPLASTIC COMPOSITES USING AUTOMATED FIBER PLACEMENT

ÖZKAN OKAN

MANUFACTURING ENGINEERING MSc. THESIS, JULY 2022

Thesis Supervisor: Prof. Dr. BAHATTİN KOÇ

Keywords: Additive Manufacturing, Automated Fiber Placement, Stiction, Hybrid Manufacturing

Increasing use of composites in load-bearing structures brought new challenges and opportunities in design and manufacturing of automotive and aerospace parts. Recent advancements in additive manufacturing processes and developments in thermoplastic composites field present alternatives to conventional joining methods such as bolting and riveting for same or dissimilar materials. This thesis presents a novel method of joining carbon fiber reinforced polymer (CFRP) composites to additively manufactured metals, without the need of fasteners or adhesives. Metal substrates with hierarchical surface protrusions in their bonding zones are designed and manufactured using laser powder bed fusion process. Using automated fiber placement, thermoplastic carbon-fiber composites are manufactured on top of the additively manufactured metal substrates with the protrusions to form a hybrid metal-composite junction. Several protrusion patterns and configurations are evaluated in terms of apparent shear strength in single lap shear tests per ASTM-D-5868. Surface properties of the as-manufactured metal specimens are evaluated and their effects on joint strength are investigated. It is demonstrated that the hybrid joints formed with this method present a viable alternative to mechanical or adhesive joining.

ÖZET

EKLEMELİ ÜRETİLMİŞ, PATERNLİ METAL ARAYÜZLER İLE TERMOPLASTİK KOMPOZİTLERİN OTOMATİK FİBER SERME METODUYLA BİRLEŞTİRİLMESİ

ÖZKAN OKAN

ÜRETİM MÜHENDİSLİĞİ YÜKSEK LİSANS TEZİ, TEMMUZ 2022

Tez Danışmanı: Prof. Dr. BAHATTİN KOÇ

Anahtar Kelimeler: Eklemeli İmalat, Otomatik Fiber Serme, Yapışma, Hibrit Üretim

Otomotiv ve havacılık uygulamalarında yük taşıyıcı yapısal elemanlarda kompozit malzemelerin kullanımı artmakta, bu durum tasarım ve üretim süreçlerinde yeni problemler ve fırsatlar yaratmaktadır. Eklemeli imalat proseslerinde yaşanan gelişmeler ve termoplastik kompozitler alanında gerçekleşen ilerlemeler, farklı veya aynı tür malzemelerin bağlanması için kullanılan geleneksel yöntemler olan cıvata ve perçin uygulamalarına alternatif oluşturmaktadır. Bu tez çalışmasında, karbon fiber takviyeli polimer kompozitler ile eklemeli üretilmiş metal parçaların bağlayıcı ve yapıştırıcı kullanılmadan birleştirilmesi için yeni bir metot sunulmaktadır. Hiyerarşik yüzey çıkıntılarına sahip metal parçalar tasarlanmış ve lazer toz yatağı ergitme metoduyla üretilmiştir. Eklemeli üretilen özel çıkıntılara sahip metal parçaların üzerine, otomatik fiber serim metodu kullanılarak termoplastik karbonfiber kompozit serimi yapılarak hibrit metal-kompozit birleşimi sağlanmıştır. Farklı çıkıntı geometrileri ve yerleşimleriyle elde edilen kesme dayanımları ASTM-D-5868 standardına göre icra edilen çekme testleri ile ölçülmüştür. Metal parçalar için ergitme prosesi sonrasında yüzey pürüzlülüğü ölçümleri yapılmış ve yüzey kalitesinin çekme dayanımına etkisi incelenmiştir. Bu yöntemle üretilen hibrit bağlantıların bağlayıcı ve yapışkan kullanılarak elde edilen metal-kompozit bağlantılara alternatif olabileceği gösterilmiştir.

ACKNOWLEDGEMENTS

I have received a great deal of assistance in creation of this thesis, from inception of the topic to execution of the smallest details.

First and foremost, I thank my thesis advisor Prof. Dr. Bahattin Koç for his patience throughout my studies. I was able to navigate around many obstacles that have come our way thanks to the insight and guidance he has generously provided.

I thank Dr. Murat Işık for guiding me through the challenges of academia.

It is thanks to the SUIMC team that the content within this work was able to be created. I thank Ragıp Orkun Seçer, Ertan Acar, Ömer Altıntaş, Fatih Polat, Büşra Taşçı, Nergiz İlhami Mert, Turgay Gönül, Bora Gönül, Serkan Akgün and Mehmet Olcaz for their support.

Thanks to Faraz Tehranizadeh and Amin Bagherzadeh for helping me with the imaging of my samples.

I thank Ali Doğan from ARK Kalıp Tel Erozyon for his services and support.

Special thanks to Yeşim Başol Erbektaş and Turkish Aerospace for their permission to use thermoplastic raw material along with the heating pads.

All that is gold does not glitter
Not all those who wander are lost
J.R.R. Tolkien

TABLE OF CONTENTS

LIST OF TABLES

LIST OF FIGURES

1. INTRODUCTION

Carbon fiber reinforced polymers (CFRP) have been widely accepted as a high strength replacement for conventionally metal parts in industries such as aviation and automotive. Composites offer high strength to weight ratio and therefore are commonly used in structural parts. However, the manufacturing processes for composites are often costly and metals offer higher ductility and impact resistance than carbon-fiber composites.

In some applications, there is a strong the need to join the composite and metal parts together. On an airplane, for instance, composite skin panels of the wings are connected to aluminum spars and ribs. The two prominent methods for joining metals to composites are mechanical fastening and adhesive bonding. Mechanical fastening is achieved by use of fasteners such as bolts or rivets. With mechanical fastening, the joined parts are easily disassembled for inspection or repairs and no special surface treatment is necessary. This process; however, requires holes to be drilled into the CFRP. Extra design measures then need to be taken to account for the loss of strength around the hole due to fiber discontinuity and stress concentration. Often the way to negate the effects is to make composites in the assembly thicker. Combined with the weight of the fasteners, the resulting heavier structure cannot fully benefit from weight savings from choosing composites over metal skins.

Another method to establish mechanical connection between the two adherent parts is to use adhesives. Adhesives can be applied to similar or dissimilar material pairs of adherents and provide a uniform stress distribution through the bond line as opposed to stress concentration in mechanical fastening. Disadvantages for adhesive bonding are the long cure cycle of the adhesive and the need for large tooling to precisely position two -often large- parts in a non-reversible process.

Every composite part consists of a matrix and a form of reinforcement. Carbon, glass, aramid, or basalt fibers are used as the reinforcement in several forms such as single tows, woven fabrics or chopped fibers. The preferred reinforcement for structural parts in aerospace has been continuous carbon fibers in a woven fabric form, due to higher strength compared to glass and aramids. Two tracks at matrix selection for carbon-fiber composites are thermosets and thermoplastics. The names define the processibility of the material as the temperature is changed. A polymer that becomes plastic and flows upon heating is thermoplastic, whereas thermosets undergo a chemical reaction in a heating process named curing which sets the form irreversibly (Rennie, 1999). Thus, thermoplastics are repairable and weldable. This makes them a worthy candidate in composites manufacturing as opposed to the waste of material and energy in thermoset manufacturing where re-cycling the materials and energy spent for curing in an autoclave is not usually feasible.

Several emerging methods try to combine the benefits of mechanical fastening, adhesive joining and thermomechanical joining. In this direction, metal surfaces that are meant to bond with the polymeric part in a welding scheme are modified topologically to enhance mechanical interlocking as well as polymer entanglement for better joint strength. The work of this thesis lies among this group of research, where additively manufactured metal substrates with hierarchical surface topologies are joined with fiber reinforced thermoplastics via automated fiber placement. To achieve this, metal parts with micro protrusions on bonding surface are manufactured via laser powder bed fusion (L-PBF) process. Single lap shear tests are conducted to assess bond strength.

2. LITERATURE REVIEW

2.1 Additive Manufacturing

In this section, a brief history and state of the art for additive manufacturing (AM) technologies that made this thesis work possible will be presented.
The emergence of additive manufacturing technology dates back to early 80's under the name "Rapid Prototyping". Rapid prototyping offered the means to realize three-dimensional parts, free of the limitations of conventional manufacturing methods such as machining. The challenge to manufacture reliable and cost-efficient parts with additive manufacturing has been undertaken by many parties for decades. Industrial use of this new technology has been limited to scientists, doctors and artists for a long time (Wong & Hernandez, 2012). Optimization-driven sectors such as aerospace and automotive lead the work on maximizing the benefits of additive manufacturing via gaining mass-production capability.

2.1.1 Powder Bed Fusion

Powder bed fusion (PBF) is an additive manufacturing process which produces metallic components from powders layer by layer. The technology was patented in 1997 in Germany by F & S Stereolithographietechnik GmbH, granted in 1998 (Meiners, Wissenbach & Gasser, 1998). Several companies have developed PBF machines and different trademarks and acronyms exist in the market such as Selective laser melting (SLM), direct metal laser sintering (DMLS) and electron beam melting (EBM). In principle, a PBF machine lays down a certain thickness of metallic powder onto a workspace and an energy source focuses on the specific

coordinates to locally melt the powder. As the molten metal consolidates, a layer of the metallic part is formed. The machine lowers the part and re-coats the surface with a new layer of powder, and this process repeats until the part is completely manufactured. The schematic is presented in Figure 2.1.

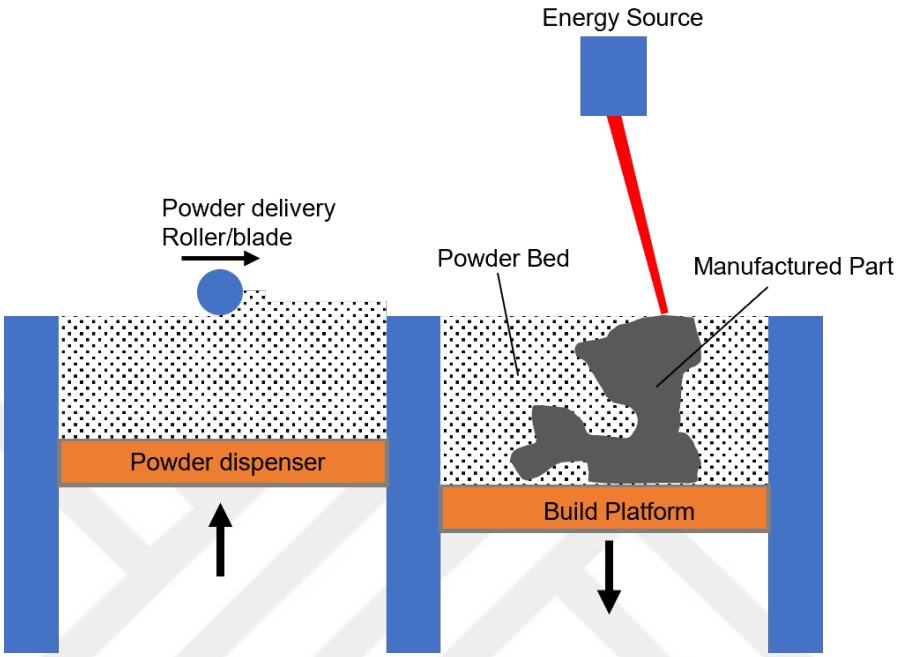

Figure 2.1 PBF process schematic

As an emerging technology in manufacturing, metal additive manufacturing is first employed for pilot studies in collaboration with universities. Mechanical properties of AM parts and dimensional accuracy along with cost aspects of the emerging technology is evaluated as a replacement of some traditional methods or towards creation of an integrated operation where AM is utilized (Fera, Fruggiero, Lambiase & Macchiaroli, 2016).

Metal additive manufacturing allows manufacturing of complex geometries where conventional methods such as machining, forming or forging have limited capabilities. However, this freedom in the design is not immediately useful due to manufacturing limitations inherent to additive manufacturing processes (Lewandowski & Seifi, 2016). Dimensional accuracy is the first critical topic in metal AM because post-processing the parts using conventional subtractive operations to achieve required dimensional tolerances negates some of the advantages of AM. Several studies aimed to improve dimensional accuracy in additive manufacturing. Effects of manufacturing process parameters on part dimensional accuracy for stereolithography is studied by Lynn-Charney and Rosen (Lynn-Charney & Rosen, 2000). Another study by Boschetto and Bottini investigated the error mitigation in FDM process via pre-processing the CAD model with design for manufacturing

point of view to reach intended part sizes (Boschetto & Bottini, 2016). On the metal AM scene, Beraud et al. proposed a new strategy to reduce the curling effect in electron beam melting (EBM) process, caused by thermal gradients within the part during manufacturing. Conventional way to eliminate thermal effects is to manufacture support structures which dissipate heat better than the powder while mechanically supporting the part against the build plate. However, these supports cause residual stress within the part and need removal after manufacturing which decreases the surface quality while increasing manufacturing complexity, time and cost. Authors showed that via modulation of beam energy depending on the surroundings of the site, better flatness is achieved in experimental production (Beraud, Vignat, Villeneuve & Dendievel, 2014).

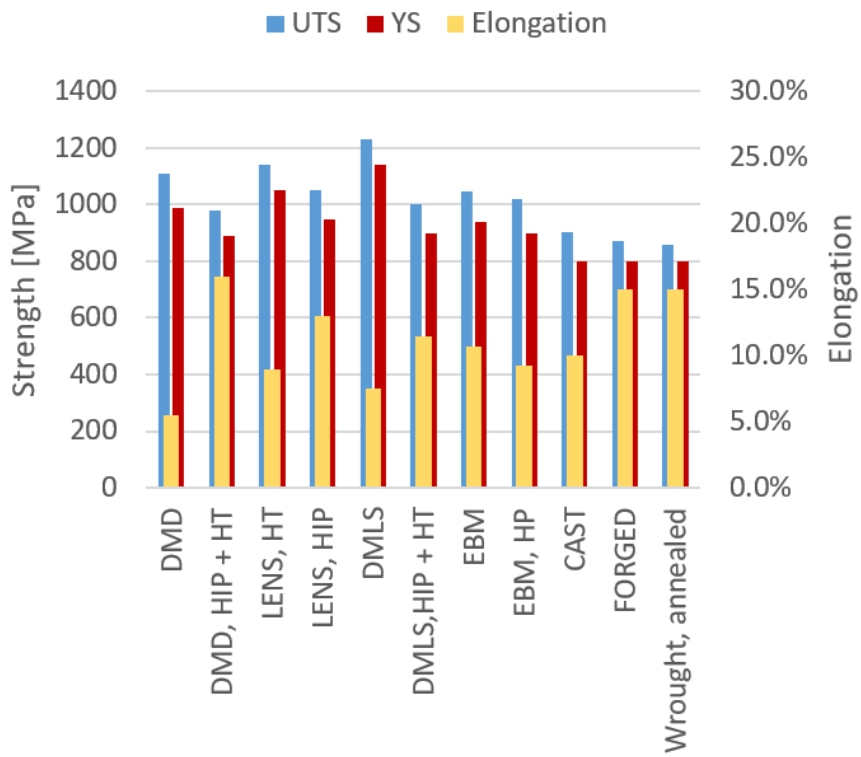

Figure 2.2 Ti6Al4V mechanical properties comparison (redrawn from Dutta & Froes (2016))

Another critical property for AM metal parts is their mechanical properties in comparison to machined counterparts. Additive manufacturing of metals rely on the liquefaction and solidification of the material, similar to conventional casting and welding processes. Thus, the issues existing with these processes are also inherited by additive manufacturing, such as porosity and directionally differing properties. Most extensive work in this field is conducted on titanium alloy Ti6Al4V, also called

Ti64, which is a workhorse in aviation industry. It is evident from literature that additively manufactured titanium exhibits better tensile strength in comparison to cast, forged and wrought states as seen in Figure 2.2. The review by Lewandowski & Seifi is a comprehensive source that gathers various studies on material properties for AM metallic parts. It is shown that direct metal laser sintering (DMLS) manufactures parts with higher ultimate tensile stress values compared to electron beam melting (Lewandowski & Seifi, 2016). In terms of directionality, a study by Rafi et al. reports that ultimate tensile strength of coupons manufactured in vertical (build) direction for Ti64 is marginally lower than those of horizontally built, with 1219MPa and 1269MPa respectively (Rafi, Nadimpalli, Gong, Starr & Stucker, 2013). Standardized strength values are not yet available for AM parts in comparison to conventional metals that are produced in the form of plates, sheets or rods where specifications such as AMS for aluminum alloys are well defined. Thus, as is the case with composites, AM metallic parts require extra steps in qualification such as coupon tests to validate the expected mechanical strength. With standardization of AM processes and availability of more data, it is expected that AM specifications will increase.

2.1.2 Automated Fiber Placement

The benefits of manufacturing carbon composite parts via automated processes were evident shortly after the development of commercially usable carbon fiber materials in 1966 (Dorey, 1987). Two processes that are prominent in this direction are automated tape laying (ATL) and automated fiber placement (AFP) (Brasington, Sacco, Halbritter, Wehbe & Harik, 2021). ATL is a process where traditional hand layup methods are replicated by a programmable configuration. This allows fast laying of uni-directional (UD) tapes of width 75-300 mm, on relatively flat surfaces. ATL is utilized with high layup speeds especially on larger parts. AFP is a more refined application of the same philosophy, where a laying head connected to a gantry or robotic arm configuration places strips of composite material called tows onto a tool surface. AFP tows range from 6.35 mm to 25.4 mm in width, allowing better steering than ATL in higher complexity parts. Process schematic is presented in Figure 2.3. ATL and AFP offered great reduction in production times by speeding up the layup of prepregs but thermoset parts required to go through autoclave process to be cured. With larger parts, the investment for large autoclave facilities becomes a driving concern. Preliminary work on in-situ ultraviolet curing for thermoset composites in AFP processes is conducted by Abulizi et al. It is shown that in-situ UV

curing for thermosets in an AFP setup is a cost efficient novel method against the autoclave process but difficulties in delivered resin content and weaker inter-laminar strength compared to thermal curing are its shortcomings (Abulizi, Duan, Li & Lu, 2011). Further studies on in-situ UV curing tried to optimize UV parameters and revealed that inter-laminar shear strength and curing uniformity are inversely proportional (Zhang, Duan, Zhao & Li, 2015). Lastly, a promising study on UV curing presented better properties in comparison to traditional methods such as infusion, however it is conducted using a conventional press configuration and an optimized process is not yet available for AFP (G. Pérez-de Eulate, Iztueta, Gondra & Vallejo, 2020). A great advantage of manufacturing composites with additive manufacturing methods is that the parts are service ready after manufacturing. Achieving this requires in-situ curing or consolidation, an area in which thermoplastic manufacturing processes offer greater maturity in comparison to thermosets where out-of-autoclave (OoA) processes exist but curing times are long.

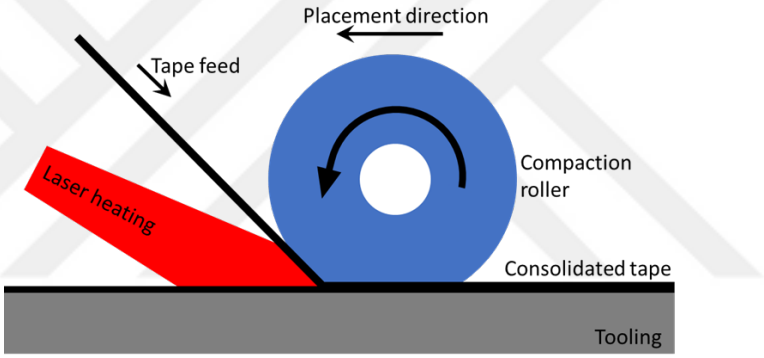

Figure 2.3 AFP process schematic

The inter-laminar strength of a composite layup is of great importance due to high transverse shear loads. Combined with the risks from imperfections in manufacturing such as gaps, voids and overlaps, delamination is a major failure mode for composites. To ensure adhesion in between the layers, AFP process utilizes a compaction roller together with a heat source that applies pressure as well as heat to ensure inter-laminar bonding while reducing the voids within the parts. The heat source is typically referred as "heater" and is critical in adhesion between the incoming tows and the substrate (Brasington et al., 2021). Several methods used are hot gas torches, infrared, laser and pulsed light heating. Early systems used hot gas torches with low energetic efficiency and infrared sources lack the required power intensity required at the nip point. The most commonly used heater is diode lasers with high controllability and temperature (Martin, del Castillo, Fernandez & Güemes, 2020).

2.2 Hybrid Joints

Literature on joining of metals and composites to form "hybrid joints" has been growing since early 2000s. The first alternative to mechanical joining methods such as bolts and rivets is adhesive joining. Almost every material combination can be joined by the use of adhesives, however this method comes with its own challenges and inefficiencies. The mechanism of adhesion and literature is presented in Section 2.2.1. Research work that are in association with automotive industry focus on fast, repeatable, and cost-effective methods that are suitable for high volume manufacturing. To achieve this, great effort has been put into process optimization for thermomechanical joining methods. Literature on joining of dissimilar materials via thermomechanical processes are detailed in Section 2.2.2.

2.2.1 Adhesive Joining

Adhesion is a phenomena that can be investigated in theoretical and practical sense (Pocius, 1986). This work is focused on the practical side that defines the strength of two adherents via mechanical testing. Among the three theories of adhesion laid out by Pocius, wettability/adsorption theory and mechanical interlocking theory are of greatest importance for the scope of this work.
Wettability/adsorption theory evaluates the adhesive properties from thermodynamics point of view. For an adhesive bond to develop, the metal surface needs to be wetted by the adhesive agent. The equilibrium of surface energies for the liquid with its vapor pressure, atmospheric air and metal surface yields the Young-Dupre Equation given below, where W_A^{REAL} defines the work of adhesion, γ_{LV} is the surface energy of the liquid in equilibrium with its vapor and θ is the contact angle of the liquid droplet as shown in Figure 2.4 (Pocius, 1986).

$$W_A^{REAL} = \gamma_{LV}(1 + cos\theta) \tag{2.1}$$

As equation 2.1 implies, lower values of contact angle, which constitute to higher adhesive forces to the surface in comparison to cohesive forces within the fluid, correspond to higher work of adhesion: wetting is easier and adhesive strength should be greater. It is also experimentally shown that the work of adhesion is

directly related to adhesion strength. Barbarisi showed for an epoxy adhesive on polyethylene that there is a linear relationship between the tensile shear strength and $(1+cos\theta)$ (Barbarisi, 1967).

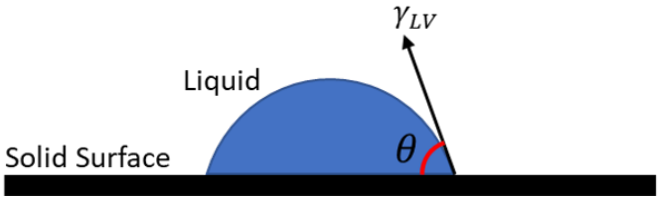

Figure 2.4 Contact angle schematic

Mechanical interlocking theory for adhesives explains the intuitive approach that more surface features in forms of roughness contributes to higher adhesive forces. If the adherents are metal, the surface quality conventionally is from the surface roughness caused through the machining operation. For composite parts, the surface quality is a function of the mold surface quality upon which the layup is conducted. These values are generally not sufficient to ensure a high-strength adhesion between the parts and the adhesive. Thus some form of surface treatment is required to increase micro and macro roughness. On top of that, usually a corrosion inhibiting primer is applied to the surfaces to increase bond durability. A prominent factor in adhesive joint strength is the environmental conditions under which the joint needs to perform. Even with intensive preparation, adhesives exhibit in-use problems such as moisture absorption, residual shrinkage, swelling and sustained thermal and mechanical stresses. Adhesive joints typically lose their strength and fatigue resistance when exposed to environmental conditions such as humidity, salinity and temperature (Abdel Wahab, 2012). Moisture is one of the major issues in aviation since aircraft are cyclically exposed to the elements and large temperature differences. A study on FM73 adhesive showed that a 3.75% moisture content decreases the Young's modulus of the adhesive from 1650 MPa to 1400 MPa (Han, Crocombe, Anwar, Hu & Li, 2014). Therefore, the sizing of the adhesive joint should be done conservatively to account for the performance deficit due to environmental factors. This conservatism leads to extra weight for the final assembly. Failure modes of adhesive joints are also important in joint design. Optimally, a joint which yields is preferred to avoid sudden loss of performance as observed in brittle adhesive joints to allow for fault detection and repair. To couple benefits from adhesive and mechanical joining methods, Moroni et al. conducted an extensive series of experiments on fastened-bonded joints (Moroni, Pirondi & Kleiner, 2010). It is shown that a hybrid of mechanical and adhesive joining resulted in higher ductility in the joint, increased energy absorption and overall presented a better alternative to either method used alone.

The availability of adhesives for thermoplastic composites is scarce, since thermoplastics are inherently capable of forming melts to achieve required bonding interface. Most adhesives formulated for composites are in thermoset form and require curing cycles at elevated temperatures. Strength values taken from manufacturer data sheets for some commercially available adhesives used for thermoplastic composites are given in Table 2.1. These values are used as a benchmark to compare the added strength via additively manufactured special surface protrusions. Note that these values do not include the effects of moisture.

Table 2.1 Commercially available adhesive properties

Adhesive Name	Test Method	Test Temp.	Adherent Substrate	Ultimate Strength
Solvay FM®377S	Lap Shear ASTM D 1002	24°C	2024-T3 Aluminum	21.5 MPa
3M DP6310NS	Overlap Shear EN 2243-1	23°C	Carbonfiber Epoxy	22 MPa
3M DP190*	Single Lap Shear (Block Shear)	N/A	Mitsubishi NB-EP4030	9 MPa (20 MPa)
3M 7246-2 B/A FST	Overlap Shear EN 2243-1	23°C (80°C)	2024-T3 Aluminum	8.1 MPa (7.2 MPa)

* Redmann et al. (2021)

2.2.2 Thermomechanical Joining

Thanks to the remoldable nature of thermoplastics, unlike thermosets, thermomechanical processes for joining of thermoplastic composites to metals are feasible. In a thermomechanical joining process, an external energy source such as friction, laser or ultrasonic vibration is utilized to heat the adherents up to their joining temperature range (Lambiase et al., 2021). Once the polymer is raised above its melting temperature, the applied pressure forces the molten flow to fill in the asperities on the metallic surface. Heat is applied to the bonding zone to melt polymeric material, to initiate intermolecular diffusion and entanglement of the polymer chains to form a joint (Sercer & Raos, 2010). General process schematic is given in Figure 2.5. Note that this schematic is the working principle behind many processes under thermomechanical joining category, such as spot or continuous joining via friction assisted joining, friction spot joining, ultrasonic welding or laser assisted joining.

Joint mechanism in this method can be micromechanical interlocking, chemical bonding or physical interactions while more than one mechanism is often involved

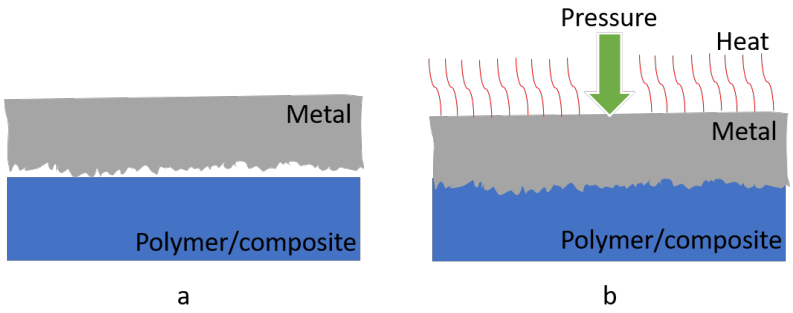

Figure 2.5 Thermomechanical joining (redrawn from Lambiase et al. (2021))

in resultant joint strength. Chemical bonding and physical interactions are the formation of covalent bonds and weaker forces such as Van der Waals or Hydrogen bonds (Lambiase et al., 2021). Using a thermomechanical joining method which has lots of parallels with welding, an established joining method for metals, is advantageous for mass-production capability in especially automotive industry. A welding process can easily be automated using industrial robots with specific end effectors such as laser heaters.

A laser joining scheme is presented in Figure 2.6. Wang et al. argue that laser joining of CFRPs to metals is superior to mechanical fastening because it avoids the risk of galvanic corrosion between steel or aluminum fasteners and electrically conductive, chemically noble carbon fibers (Wang et al., 2019). To join metals and composites via laser energy, the two adherent parts are clamped together and a laser beam is applied onto the top surface. Laser energy is absorbed by the metal and increased temperature at the interface melts the polymer. Viscous thermoplastic then re-entangles around the asperities on the treated surface, creating the bond. To enhance the interlocking process, surface preparation, clamping force and process temperature need to be optimized.

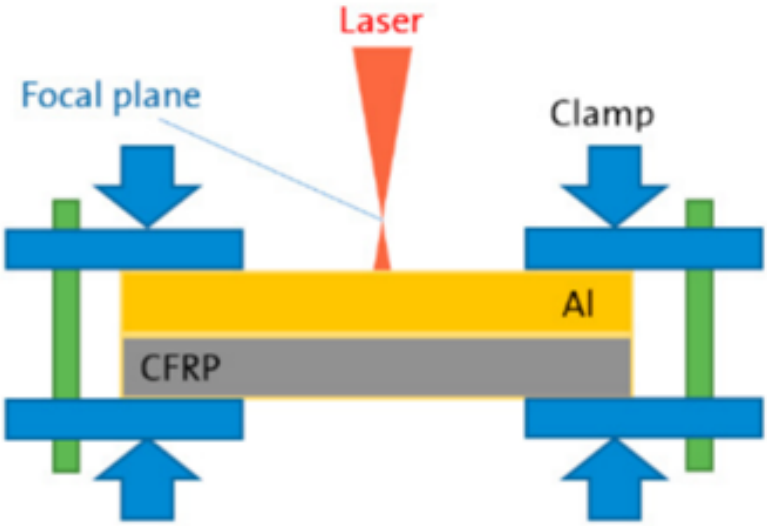

Figure 2.6 Laser joining process schematic (Wang et al., 2019)

Another method for thermomechanical joining is via utilization of ultrasonic vibration. Ultrasonic joining processes have been successfully used for joining of metal, plastic and dissimilar pairs. A mechanical device named sonotrode applies a high frequency vibration to the adherents which are clamped together by some force, as shown in Figure 2.7 (Wagner et al., 2013). Shear strengths of up to 50MPa are achievable using ultrasonic welding methods, as seen in Figure 2.8 (Amancio-Filho et al., 2011).

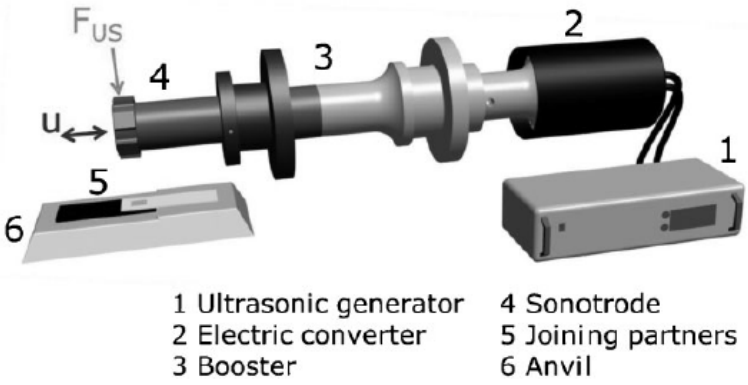

Figure 2.7 Ultrasonic spot welding scheme (Wagner et al., 2013)

However, the small amplitude and high frequency of the process means that the energy cannot be transferred to the bonding zone for thicker parts, since the upper material on which the vibration is applied absorbs too much of the energy. Therefore, this method, while very successful with materials of the sheet form, is not extendable to thicker or more complex geometries.

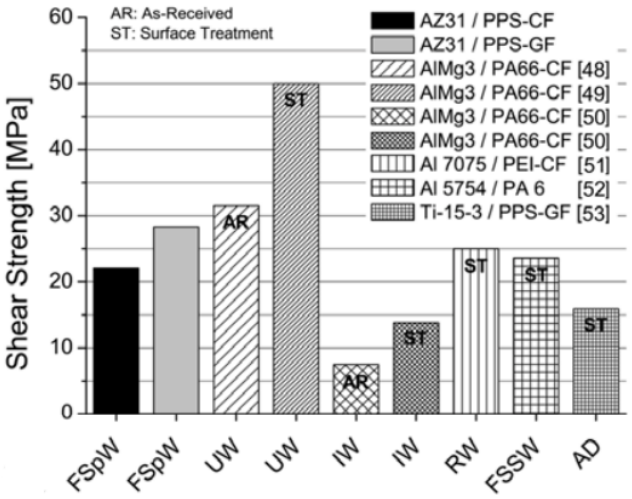

Figure 2.8 Hybrid joint strength comparison (Amancio-Filho et al., 2011)

2.2.3 Joints with Surface Modifications

A robust connection within hybrid joints is highly dependent on the surface pretreatment. Comparison of various surface treatments have been conducted and available in the literature. Molitor et al. compare mechanical, chemical, electrochemical, and energetic surface treatments are used on Ti-6Al-4V to enhance metal surface prior to bonding (Molitor, Barron & Young, 2001). It is stated that producing significant micro-roughness on the surface yields the best durability in the formed bond, followed by treatments that produce significant macro-roughness but little micro-roughness. Surface preparations with no significant micro or macro roughness are revealed to demonstrate the poorest bond durability. Chromic acid anodization and NaOH anodization create oxide layers of 40-140 nm and 80-90 nm thickness on titanium surface, respectively. Molitor et al. classify strength of bonds created with these treatments as high with excellent durability (Molitor et al., 2001).
A new approach to surface treatment of metals for hybrid joining to thermoplastics has been demonstrated by Kohl et al. (Kohl, Schricker, Bergmann, Lohse, Hertel & Füssel, 2018). A tungsten inert gas (TIG) arc process is utilized and the surface morphology and bond strength is evaluated against surfaces created via continuous wave (cw) and pulsed wave (pw) laser processes. Although the joint is found to be less strong in mechanical testing, the area output of TIG process is more than ten-fold higher than laser processes. High throughput makes this process a cost-efficient alternative since using power-intensive laser processes is infeasible for large parts (Kohl et al., 2018).

Amend et al. investigated another surface treatment in steel to polyamide hybrid joints utilizing laser cladding, an additive manufacturing process. By creating "weld lines" with heights ranging from 23 to 33 microns on steel sheet metal adherents, they have shown that the bond strength can be improved (Amend, Hentschel, Scheitler, Gorunov & Schmidt, 2015).
The surface treatments mentioned in this section are at the scale of micrometers. The processes are relying on the wetting of the micro-structures by the plastic adherent to achieve a mechanical form fitting. This approach presents advantages in improving on existing laser joining methods with untreated surfaces. However, since the joint strength is predominantly a mechanical interlocking phenomena, the methods presented in Section 2.2 produce stronger hybrid joints by utilizing interlocking between several layers of composites and the metallic adherents. As a trade-off between the two approaches, a method which utilizes surface treatment at the millimeter scale but does not require secondary joining operations such as ultrasonic welding is demonstrated in this work. To increase hybrid bonding strength via increasing the mechanical interlocking area, special surface modifications are investigated. The literature on joints with surface modifications for thermoset and thermoplastic composites are given in this section. Creating hybrid joints using thermosetting polymers bears several advantages over thermoplastic polymers. In the processes for thermoset composites, the protrusions are inserted into the dry fabric or pre-impregnated composite parts and the parts are bonded during the curing cycle of the composites. With the thermoplastics, it is possible to manufacture joints using thermomechanical joining methods and process cycles are much shorter in comparison. This translates into higher joint strengths with thermosetting composites.

2.2.3.1 Joining for Thermoset Composites

A method of creating controlled protrusions on metal adherents is named Surfi-Sculpt® developed by TWI (The Welding Institute, 2004). This patented process utilizes a relative movement between the laser beam and the workpiece to manipulate the melt pool to create desired textures on the metal specimen. Tu et al. developed a hybrid bond using Surfi-Sculpt on titanium Ti-6Al-4V alloy and pre impregnated carbon fiber composite AS4/8552 and named the process Comeld™ (Tu, Guild & Hogg, 2009). Additive manufacturing offers the means to create controlled surface protrusions. Cold Metal Transfer (CMT) developed by Fronius GmbH is a new method that achieves this goal via melting a filler wire of known height onto a metal

part in an arc welding configuration. The welding wire is teared at designated heights and several tip shapes as shown in Figure 2.9 are possible. Metal substrate with these "spikes" is then pressed into a pre-preg state thermoset composite part with help of ultrasonic vibration. The protrusions here are meant to pierce through several layers of the composite and intertwine with the fibers, forming a stronger interface between the two parts. Using this method, joint strengths of up to 21.9 MPa is achieved (Ucsnik et al., 2010).

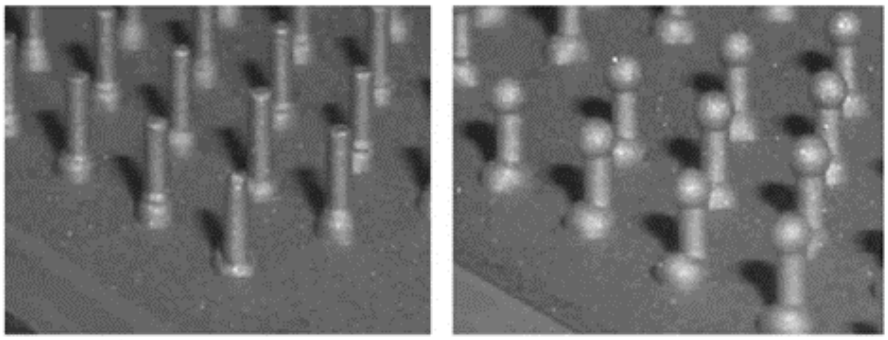

(a) Cylinder Pins (b) Ball-head Pins

Figure 2.9 CMT pins (Ucsnik et al., 2010)

Another novel method of hybrid joining called HYPER (Hybrid Penetrative Reinforcement) has been developed by Parkes et al. in cooperation with AIRBUS Group UK (Parkes, Butler, Meyer & de Oliveira, 2014). Similar to CMT, A HYPER joint consists of metal spikes on the surface which are inserted into the composite and the two parts are co-cured. This process is advantageous over the previous ones in terms of design flexibility in parts where various curvatures are present. The protrusions are manufactured via powder bed fusion which allows a broader selection of protrusion shapes. In HYPER joints, an arrowhead design shown in Figure 2.10 is utilized to prevent pullout after consolidation. It is shown that HYPER joints can achieve up to 52 MPa ultimate strength (Bianchi, 2012).

Figure 2.10 HYPER joint section view (Bianchi, 2012)

2.2.3.2 Joining for Thermoplastic Composites

Special surface textures can be created via application of energy onto the metal surface, one such method of creating surface texture is via laser ablation, as demonstrated by Amend et al. (Amend et al., 2013). Concentrated laser radiation is applied onto the surface in several passes called scans. More material is removed with each scan, giving the flexibility to create grid structures of varying depths as shown in Figure 2.11. The structured surface is connected to the thermoplastic composite using laser joining, yielding joint strengths of up to 19.7 MPa (Amend et al., 2013).

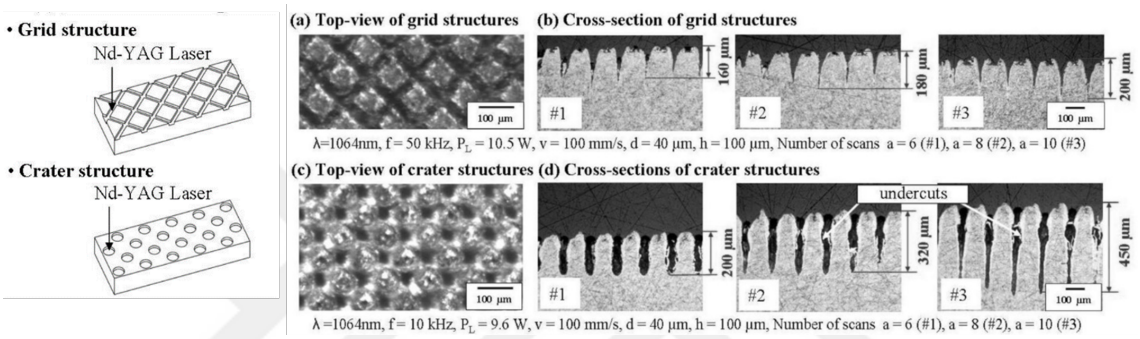

Figure 2.11 Laser structuring of aluminum surface (Amend et al., 2013)

Another patented process of joining lightweight metals whose surfaces have been created by metal injection molding process MIMStruct (Ebel, Amancio-Filho & dos Santos, 2013) to fiber reinforced polymers via an ultrasonic method called U-Joining (Amancio-Filho, Feistauer & dos Santos, 2015) is shown to be advantageous over other state-of-the-art technologies in terms of process time (Feistauer & Amancio-Filho, 2018). The load bearing behavior of the joint is evaluated via customized single lap shear tests and a significant increase in strength and damage tolerance is reported in samples with higher number of protrusions, 5.3 MPa and 7.9 MPa are reported for four and six pin joints respectively, as shown in Figure 2.12.

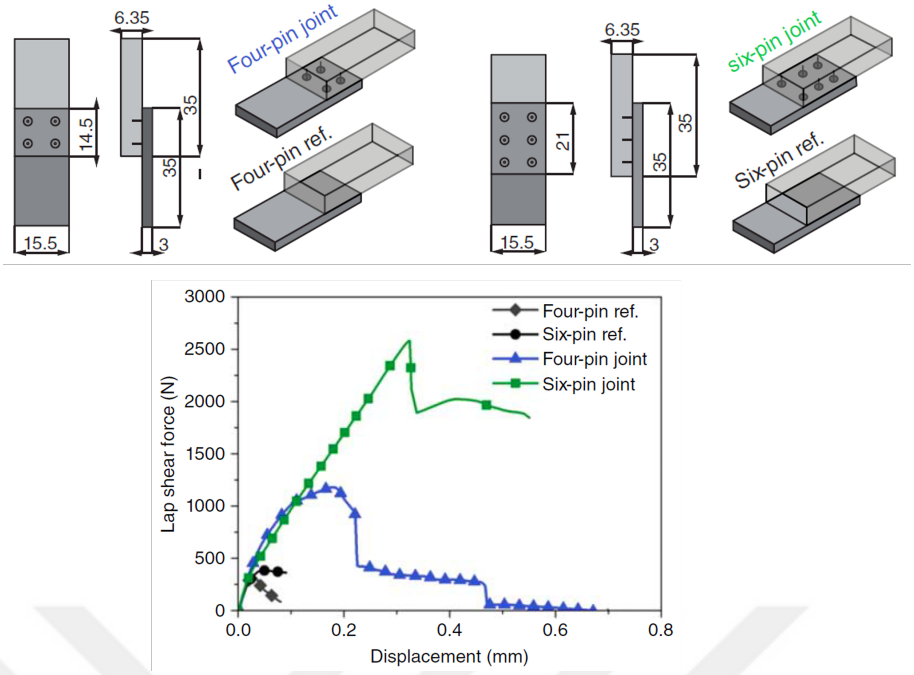

Figure 2.12 Lap shear specimens manufactured via U-Joining and test results (Feistauer & Amancio-Filho, 2018)

3. METHODOLOGY

3.1 Design & Analysis

3.1.1 Design Definition

The design objective is to manufacture an interlocking geometry between the metal and composite parts. Carbon fiber/PAEK fiber tows are laid via automated fiber placement technique onto an additively manufactured metal part with special protrusions on the surface. As the thermoplastic melts and consolidates between the protrusions, mechanical interlocking is achieved, and two dissimilar materials are connected. The process schematic is given in Figure 3.1.

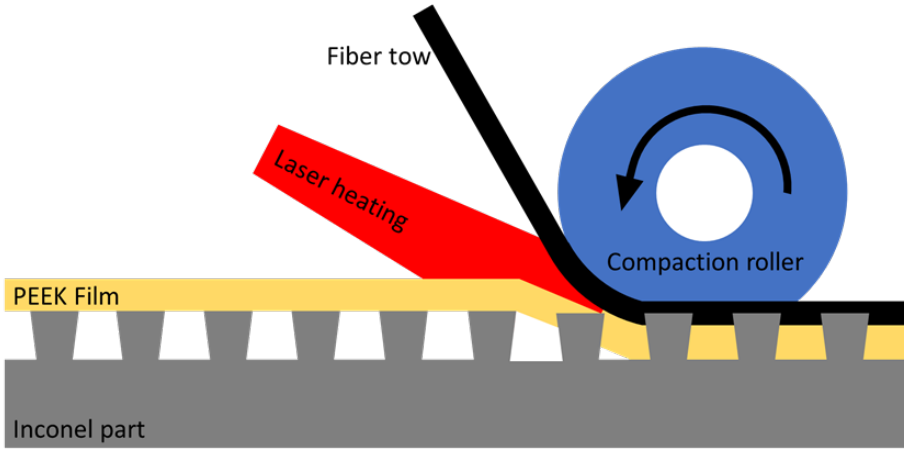

Figure 3.1 Interlocking schematic

To obtain maximum bonding strength, the geometry of a single protrusion is studied. Since the geometry is to be optimized for single-lap shear loading, the protrusion

is loaded in shear direction, assuming no bending, as seen in Figure 3.2. The goal of the optimization is to achieve highest stiffness value at the interface. To assess this, an arbitrary and constant load is applied to the CFRP as shown in Figure 3.2 while the metal part is fixed at its bottom. Height of the protrusion $h_1$is fixed at 1mm to avoid damage to the compaction roller during AFP and to ensure proper polymer filling among the protrusions without voids. R_{fillet} is determined via the imaging of manufactured samples and set as 0.09mm. The optimization algorithm modifies h_2 and α values and minimizes the average deflection on the surface where the load is applied. Overhang angle α is varied between 0 and 45 degrees to enable additive manufacturing of the protrusions without the need for support structures. h_2 is varied between 0.2 and 0.8mm. To capture material behavior at the vicinity of the corners and fillets and to avoid numerical errors, an extra-fine mesh is created as shown in Figure 3.3. The solver updates the mesh according to the changing geometry while modifying the design dimensions.

It is observed that the varied parameters for the protrusion shape are not a major factor in joint failure. Shear loading at the bottom of the protrusion is almost constant and is a factor of protrusion width. Stiffness mismatch between the metal and composite and the corner radius at the protrusion head results in local yielding of the composite as shown in Figure 3.4. The modeling complexity to accurately simulate the failure modes of the interface with dissimilar & non-homogeneous materials with large deformations is found to be overtaxing for the scope of this work. It is also discovered that the more prominent problem is the proper filling of the space between the protrusions and this analysis requires a thermal flow model with incorporated crystallization dynamics. Thus, further updates on the protrusion shape and density are conducted using the experience gained through the project.

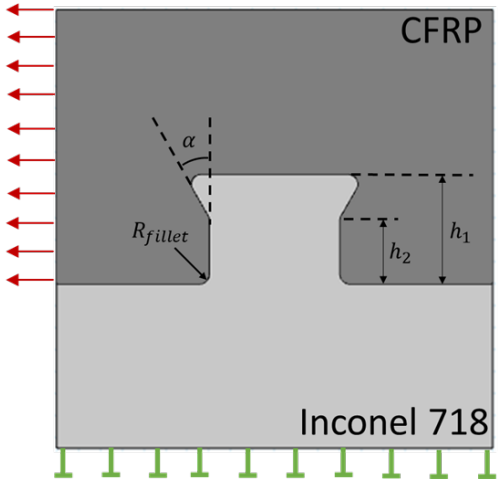

Figure 3.2 Protrusion geometry

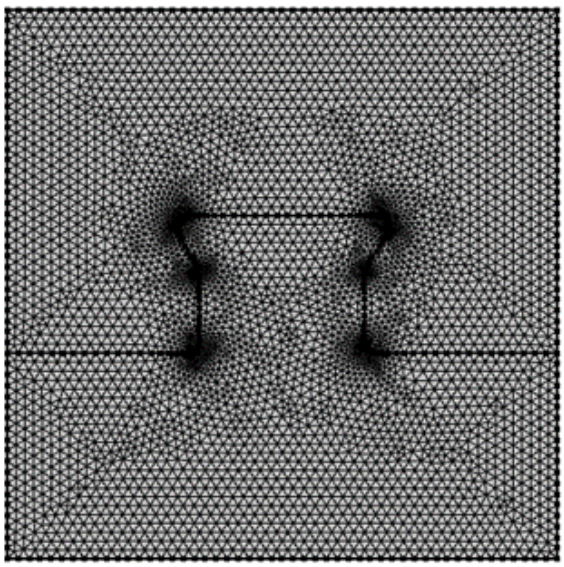

Figure 3.3 Free triangular mesh

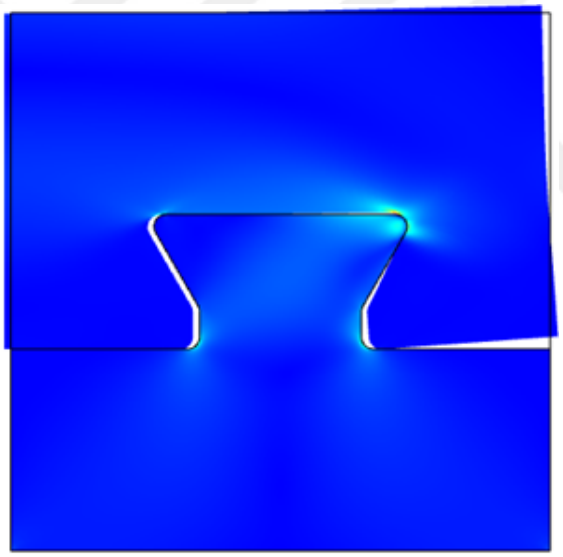

Figure 3.4 FEA stress plot

3.1.2 Analysis

3.1.2.1 Mechanical Analysis

Unlike the micro-size interfaces, the global response of the composite stack can be approximated using classical laminate theory. The hybrid bond consists of two materials from a modeling point of view: carbon fiber reinforced PAEK and Inconel 718. For the composite part of the test specimens, 17 layers of unidirectional (UD) tape has been laid to achieve 2.5mm thickness. Elasticity matrix for the composite part is deduced using classical laminate theory and fed into the simulation tools.

Table 3.1 Material properties - Composite

Material	Elastic Modulus	Poisson's Ratio	Volume Fraction
Carbon Fiber	$E_f = 228\text{GPa}$	$\nu_f = 0.22$	$f_f = 0.6$
PAEK	$E_m = 3.5\text{GPa}$	$\nu_m = 0.38$	$f_m = 0.4$

The forces [P], and moments [M] of a thin plate can be computed from the strains [ϵ], and curvatures [κ] using the stiffness between force-strain, force-curvature and moment-curvature couplings represented with [A], [B] and [D] respectively in equation 3.1.

$$\begin{Bmatrix} P \\ M \end{Bmatrix} = \begin{bmatrix} A & B \\ B & D \end{bmatrix} . \begin{Bmatrix} \epsilon \\ \kappa \end{Bmatrix} \tag{3.1}$$

To define A, B and D matrices that constitute the composite stiffness matrix, classical laminate theory is applied as follows. For a single lamina, fiber shear modulus G_f and matrix shear modulus G_f are:

$$G_f = \frac{E_f}{2(1+v_f)} \tag{3.2}$$

$$G_m = \frac{E_m}{2(1+v_m)} \tag{3.3}$$

Longitudinal elastic modulus E_{11}, with iso-strain assumption is:

$$E_{11} = f_f E_f + f_m E_m \tag{3.4}$$

Lateral elastic modulus E_{22}, with iso-stress assumption is:

$$E_{22} = (\frac{f_f}{E_f} + \frac{f_m}{E_m})^{-1} \tag{3.5}$$

Combined Poisson's ratio v_{12} is:

$$v_{12} = f_f v_f + f_m v_m \tag{3.6}$$

Shear modulus G_{12} for the lamina is:

$$G_{12} = (\frac{f_f}{G_f} + \frac{f_m}{G_m})^{-1} \tag{3.7}$$

Then, in-plane compliance matrix C is formed as:

$$C = \begin{bmatrix} \frac{1}{E_{11}} & -\frac{v_{12}}{E_{11}} & 0 \\ -\frac{v_{12}}{E_{11}} & \frac{1}{E_{22}} & 0 \\ 0 & 0 & \frac{1}{G_{12}} \end{bmatrix} \tag{3.8}$$

Where,

$$\begin{Bmatrix} \epsilon_1 \\ \epsilon_2 \\ \gamma_{12} \end{Bmatrix} = C \begin{Bmatrix} \sigma_1 \\ \sigma_2 \\ \sigma_{12} \end{Bmatrix} \tag{3.9}$$

In-plane stiffness matrix Q of the lamina is:

$$Q = inv(C) = \begin{bmatrix} \frac{E_{11}^2}{E_{11} - v_{12}E_{22}} & -\frac{v_{12}E_{11}E_{22}}{E_{11} - v_{12}E_{22}} & 0 \\ & \frac{E_{11}E_{22}}{E_{11} - v_{12}^2 E_{22}} & 0 \\ & & G_{12} \end{bmatrix} \tag{3.10}$$

The strains at the reference frame should be transferred to lamina reference using transformation matrix T:

$$T = \begin{bmatrix} cos^2\theta & sin^2\theta & -2cos\theta sin\theta \\ sin^2\theta & cos^2\theta & 2cos\theta sin\theta \\ cos\theta sin\theta & cos\theta sin\theta & cos^2\theta - sin^2\theta \end{bmatrix} \tag{3.11}$$

For the UD laminate in this work, the transformation matrix is equal to identity matrix since $\theta = 0$. Thus, transformed elasticity is referred as reduced stiffness matrix, $\overline{Q}$:

$$\overline{Q} = T^{-1}QT^{-T} = Q \tag{3.12}$$

Then, A, B and D matrices for composite stiffness matrix for a layup as shown in Figure 3.5 are calculated via equations 3.13, 3.14 and 3.16:

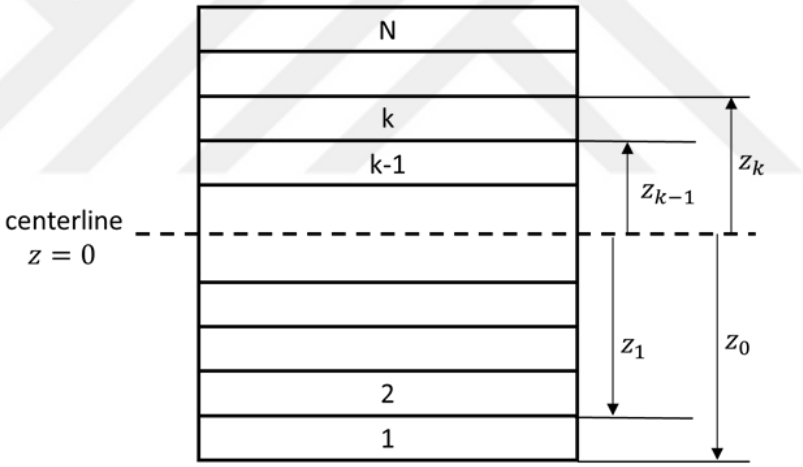

Figure 3.5 Cross-section of an N-layer composite laminate

$$[A] = \sum_{k=1}^{N} \overline{Q}_k(z_k - z_{k-1}) \tag{3.13}$$

$$[B] = \frac{1}{2}\sum_{k=1}^{N} \overline{Q}_k(z_k^2 - z_{k-1}^2) \tag{3.14}$$

$$[D] = \frac{1}{3}\sum_{k=1}^{N} \overline{Q}_k(z_k^3 - z_{k-1}^3) \tag{3.15}$$

The stiffness matrix for the 17-layer layup of this work is thus calculated as:

$$CSM = \begin{bmatrix} 299.8 & 5.27 & 0 & 0 & 0 & 0 \\ & 18.59 & 0 & 0 & 0 & 0 \\ & & 6.71 & 0 & 0 & 0 \\ & & & 116.5 & 2.05 & 0 \\ & SYM. & & & 7.21 & 0 \\ & & & & & 2.61 \end{bmatrix} \tag{3.16}$$

Mechanical properties of Inconel 718 alloy used in this work are obtained from Zhang et al. (Zhang, Niu, Cao & Liu, 2015) and presented in Table 3.2.

Table 3.2 Material properties - IN 718

Property	Value
Yield Strength	849 MPa
Ultimate Tensile Strength	1126 MPa
Elongation (%)	22.8
Hardness (HRC)	32.5
Young's Modulus	200 GPa

To evaluate shear modulus and the ultimate strength of the bond area, a simple spring-in-series approach is taken as shown in Figure 3.6. The test provides force vs displacement data from the test machine. The displacement in question includes the elongation of the adherents under tensile loading and the shear strain at the bond area. Under quasi-static assumption where inertial effects and weight of the specimens are neglected, the tensile stress causes the same reaction pair at every cross-section throughout the specimens. Using the elasticity values for 17-ply composite and Inconel 718 previously defined and the lengths from the test setup, shear deformation of the joint zone can be calculated.

$$E = \frac{\sigma}{\epsilon} \tag{3.17}$$

$$\sigma = \frac{F_{test}}{A_{specimen}} \tag{3.18}$$

$$\epsilon = \frac{L_{test} - L_{init}}{L_{init}} \tag{3.19}$$

Where,

E	Young's modulus
σ	Tensile stress
ϵ	Tensile strain
F_{test}	The load during lap shear test
$A_{specimen}$	Cross-sectional area of the specimens in pulling direction
L_{test}	Length of the specimens under load
L_{init}	Initial distance between the end of the gripper and bonding zone

Re-arranging to solve for length change of the adherents during the test, tensile elongation values at non-bonding sections of the specimens are calculated as:

$$\Delta L = L_{init} \frac{F_{test}}{A_{specimen} E} \tag{3.20}$$

Young's moduli for the metal and composite are $E_{IN718} = 200GPa$ and $E_{comp} = 299.8GPa$. Cross-sectional areas at the non-bonding regions are $A_{IN718} = 25.4 * 1.4 = 35.56mm^2$ and $A_{comp} = 25.4 * 2.6 = 66.04mm^2$. Finally, the distances between the grippers of the test machine and the bond zone are $L_{IN718} = L_{comp} = 40mm$ while the length of the bonded region L_{bond} is $25.4mm$.

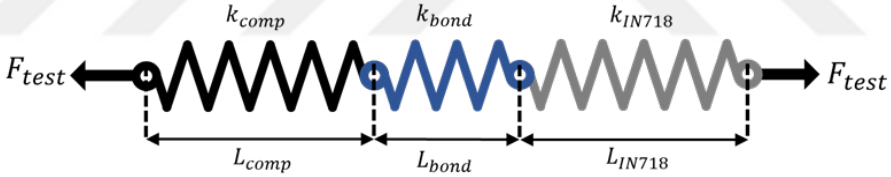

Figure 3.6 Equivalent stiffness schematic for single lap shear testing

Then to define ΔL_{bond} which is used in shear strain calculation, ΔL_{comp} and ΔL_{IN718}values are subtracted from total extension distance recorded by the test bench. Elongation of the specimens are calculated to constitute 10-15% of the total elongation for the elastic region and therefore are significant.

Figure 3.7 Shear strain definition

Shear strain γ is calculated as shown in equation 3.21, while h values are taken as

the protrusion heights measured via microscopy for each batch.

$$\gamma = \frac{\Delta L_{bond}}{h} \tag{3.21}$$

3.1.2.2 Thermal Analysis

To evaluate the flowability of thermoplastic resin, a 1D thermal model of the AFP process is developed as shown in Figure 3.8. A total of 17 layers are laid using AFP to reach a composite thickness of 2.5mm. The laser source heated the incoming tape and the top surface of previously laid tape to 400°C. The fixture is heated from the bottom and surface of the metal part is kept at a steady 180°C. Properties for the used PAEK thermoplastic tape are given in Table 3.3.

Table 3.3 Neat resin properties

Temperature		Value
Glass Transition	T_g	147°C
Melt	T_m	305°C
Crystallinity	T_c	263°C
Processing	T_p	$340 - 385$°C

Through thickness thermal conductivity of a similar material is found to be 1.338 W/m/K in literature (Perrin, Senoussaoui, Dubief & Vaudemont, 2021). Specific heat capacity of the composite is estimated using rule of mixtures with 60% PAEK resin with Cp=1340 J/kg/K and 40% carbon fiber with Cp=800 J/kg/K. Using these properties and boundary conditions, simulations are run on COMSOL to determine the transient thermal response of the composite to the manufacturing process at each layer. The top surface of thermoplastic composite after the compaction roller has passed, is in contact with 1atm ambient air at 23ºC.

Thermal analysis with AFP parameters showed that the laser exposure is only successful at increasing 2 layers of tape above the melt temperature. Adding in the incoming hot tape for the 3$^{\text{rd}}$ layer, there is only 3 layers of processable polymer to fill between the protrusions. This is a key finding in determining the feasible protrusion height. Compaction roller cannot penetrate between the protrusions because is has a flat surface. This means that the thermoplastic filling between the protrusions is a complex squeeze flow problem. A single layer of tape is 0.125mm in thickness and 3 molten layers equate to $0.125 * 3 = 0.375$ mm. During laying of the 4$^{\text{th}}$ layer,

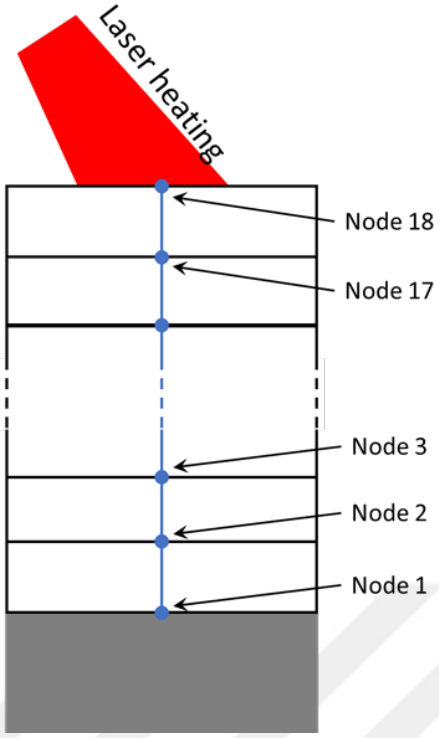

Figure 3.8 1D thermal model schematic

the temperature of the first layer has already dropped below melting temperature T_m.

The contradiction between the AFP processability and SLM manufacturability presents an iterative process refinement problem to solve. Very small protrusions that can successfully be filled in AFP are not feasible to be manufactured by SLM. A lower protrusion height means that the features at the protrusion edges that define the shape are manufactured with less resolution and accuracy. As a trade-off after the thermal analysis and experience of first two batches, the height of the protrusions are decreased to 0.6 mm for batch 3.

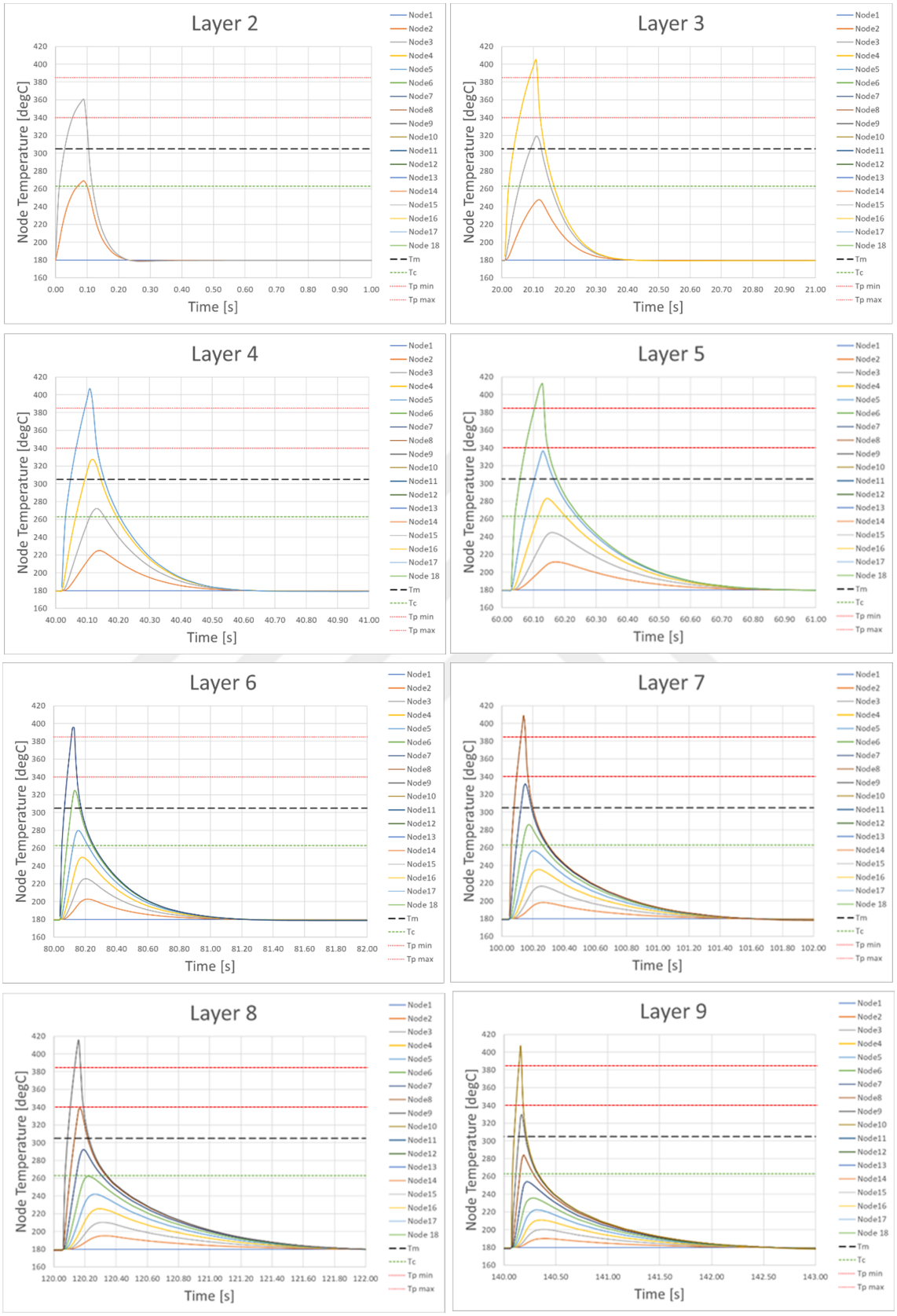

Figure 3.9 COMSOL thermal analysis results

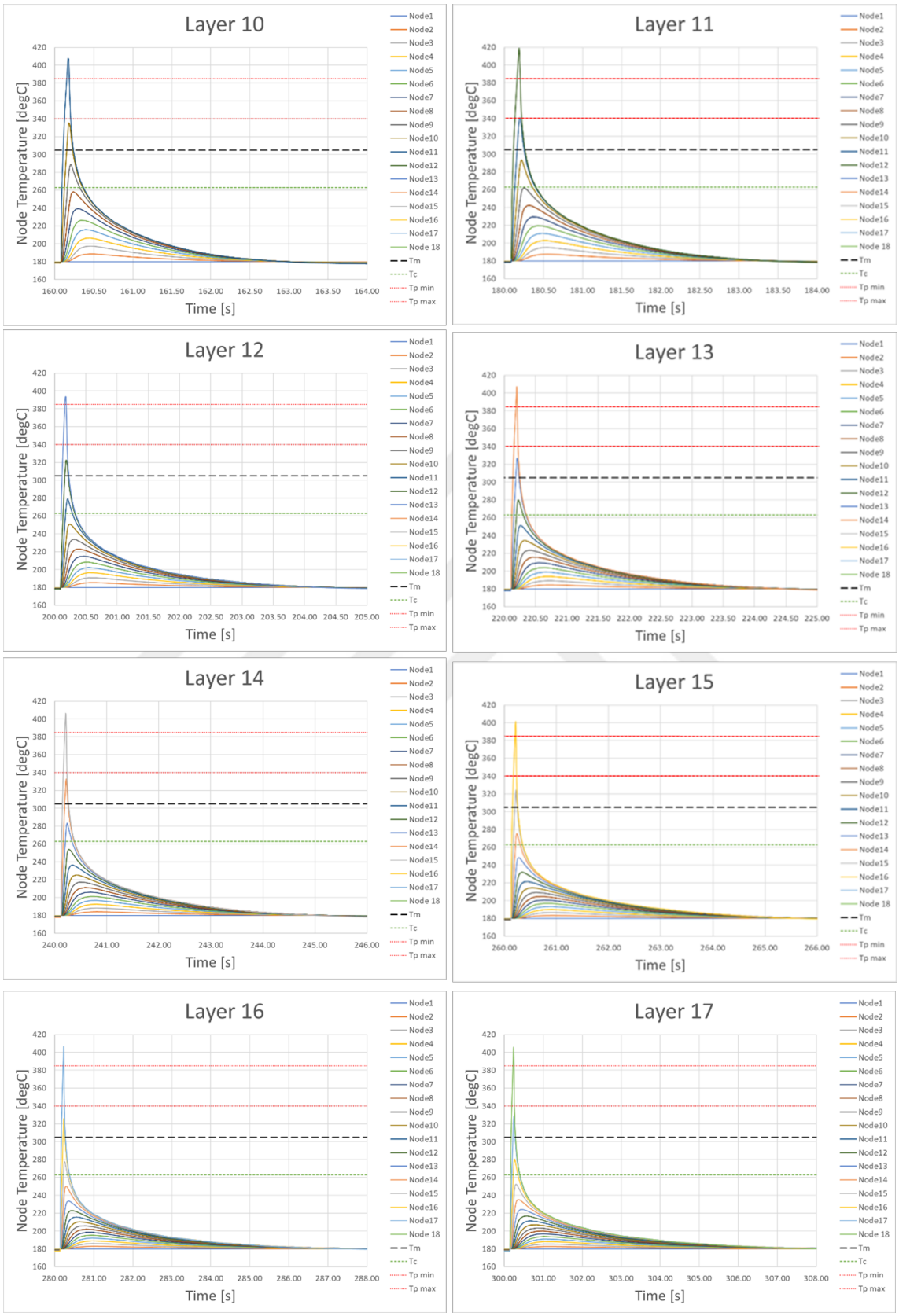

Figure 3.9 COMSOL thermal analysis results contd.

3.2 Manufacturing

3.2.1 Fixture

To standardize the manufacturing process and allow for batch production of specimens, a fixture is machined from 5083 Aluminum alloy. Four corner slots allow the fixture to be securely positioned on a standard T-slot machine bed, which allows automated fiber laying operation to be completed with high accuracy.

Figure 3.10 Aluminum fixture

Additively manufactured metal specimen which contains four coupons is placed into the slot of the fixture, leaving only the protrusions above z=0 plane as seen in Figure 3.11. This ensures the compliance with ASTM-D5868 to prevent unwanted height changes during fiber placement process. Two threaded holes for securing the specimens into the fixture via two M6 bolts is provided to avoid movement during fiber placement process.

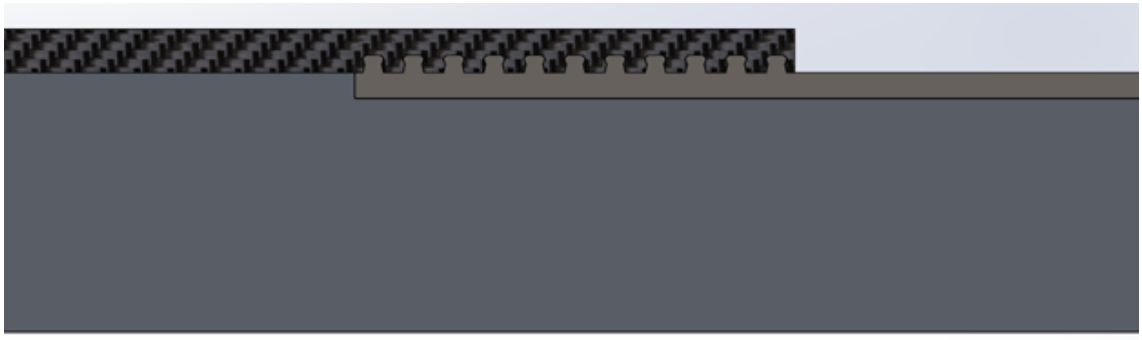

Figure 3.11 Slotted fixture cross-section

3.2.2 Metal Specimens

3.2.2.1 Powder Bed Fusion

Specimens for the tests are manufactured on EOS M290 machine. Inconel 718 alloy is used as powder material. To achieve good surface quality and minimize the staircase effect, a pre-optimized machine profile with parameters given in Table 3.4 is used throughout the project.

Table 3.4 EOS manufacturing parameters

Parameter	Value
Layer Thickness	40 μm
Laser Power	285 W
Focus Diameter	100 μm
Scan Speed	960 mm/s
Distance	11 mm
Beam Offset	15 μm
Stripe Width	10 mm
Stripes Overlap	0.12 mm
Rotation	67 deg/layer

To evaluate the effects of protrusion shape and placement, four different test specimens are manufactured in a single batch. Two shapes selected as baseline designs are given in Figure 3.12. Along with protrusion shape, to determine the effect of distribution of these micro-structures at the bond area, square and oblique placement defined as seen in Figure 3.13. Initial trials of manufacturing small sized protrusions were unsuccessful. EOS M290 is capable of manufacturing features as small as 300µm. The details finer than this value cannot be manufactured. First iteration of

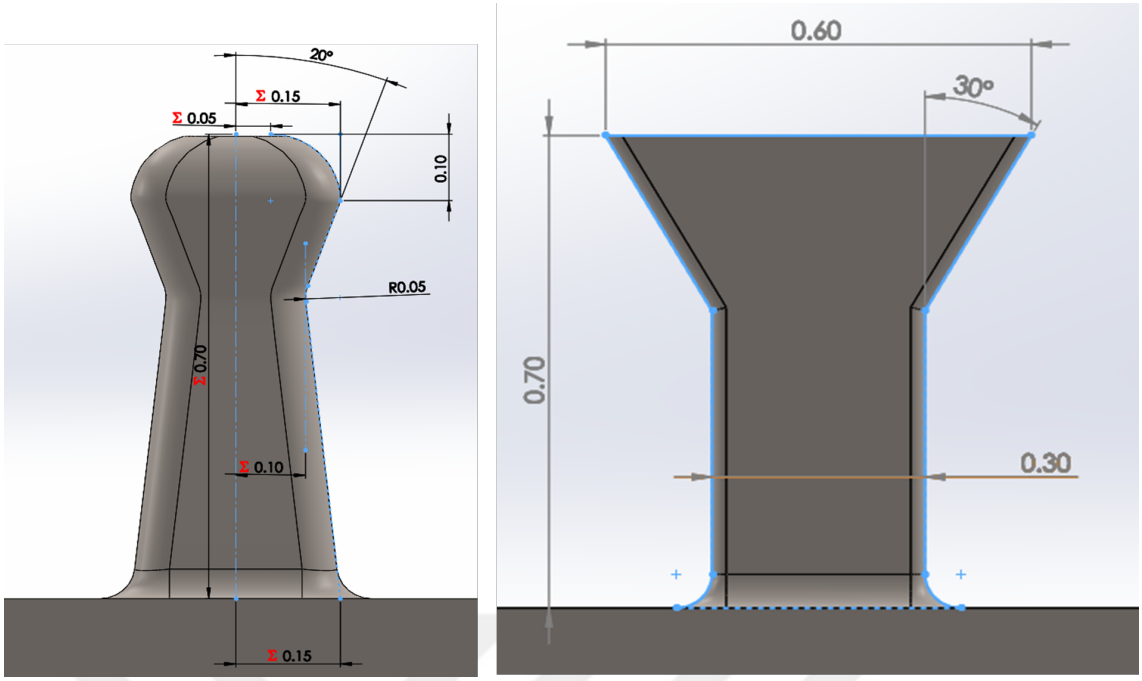

Figure 3.12 Initial protrusion sizing

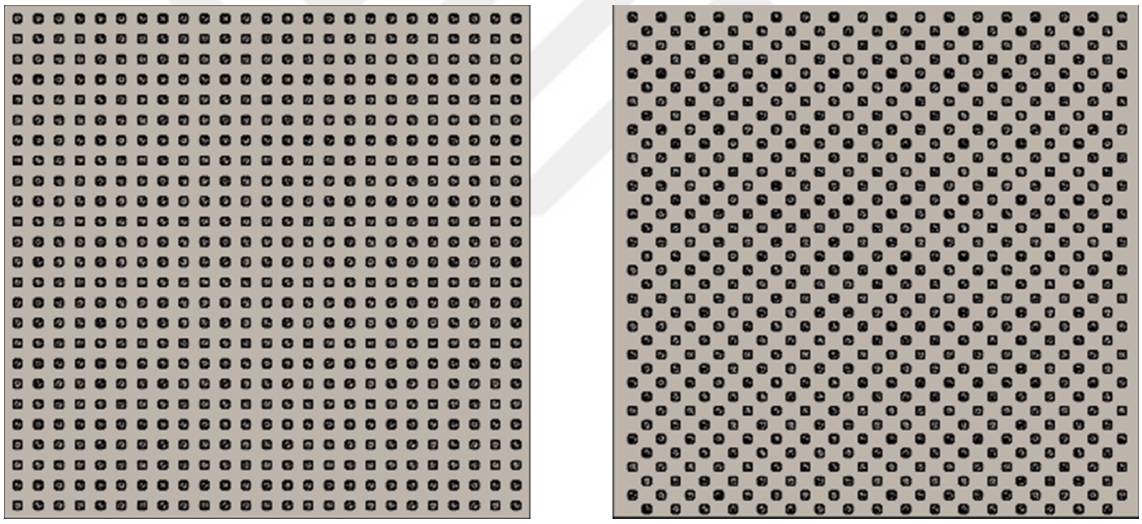

Figure 3.13 Square and oblique placement of protrusions

manufacturing which consists of the input geometries given in Figure 3.12 and 3.13 has failed. Geometry definitions for either protrusion shape in Figure 3.12 could not be observed. The microscope images for the first batch is given in Figure 3.14. Protrusion sizes are then increased as seen in Figure 3.15 and manufacturing accuracy of the specimens are deduced with microscope imaging, as shown in Figures 3.16 and 3.17.

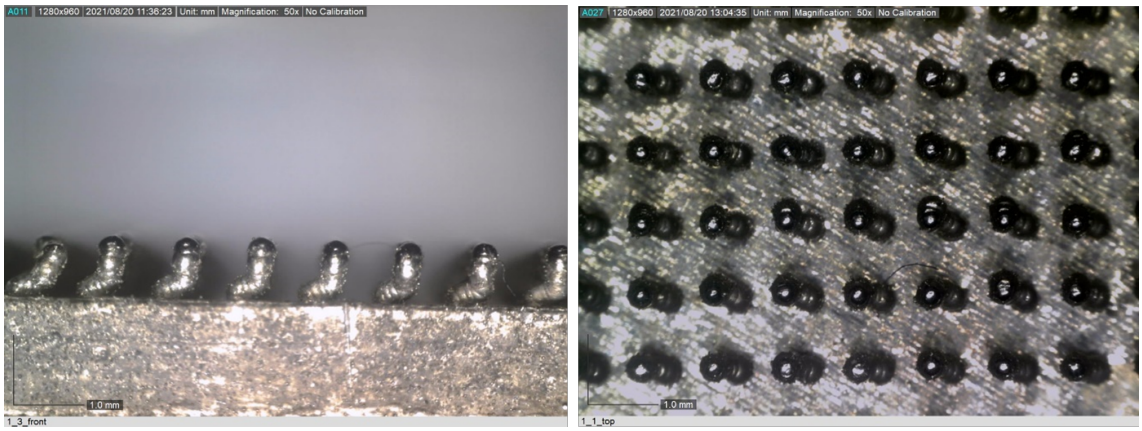

Figure 3.14 Batch 1 - Failed protrusions side and top views

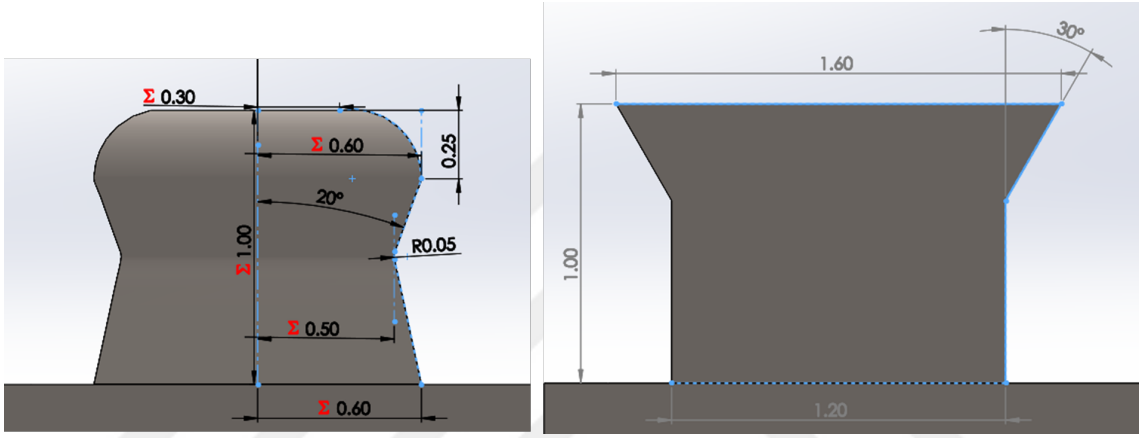

Figure 3.15 Revised protrusion sizes for Batch 2

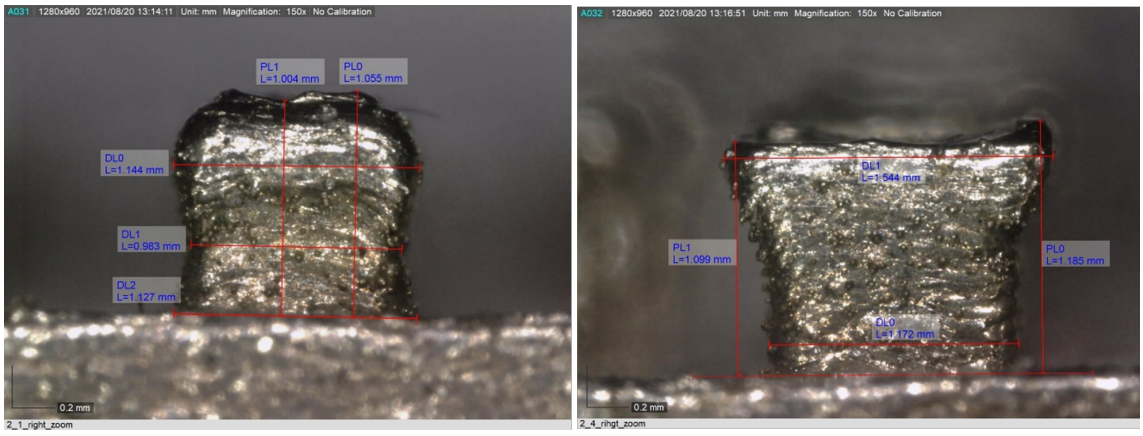

Figure 3.16 Batch 2 - Manufactured protrusion geometries

The deviation from CAD model is due to melt pool size. There were still some features which are smaller than 300um resolution limit, however an even larger protrusion is required to manufacture such geometries. This would contradict the purpose of the study of micro-protrusions and therefore the deviance from CAD data is accepted as a limit of manufacturing capabilities. Finite element analysis

models are modified to reflect the manufactured protrusion samples in terms of dimension and shape inaccuracies.

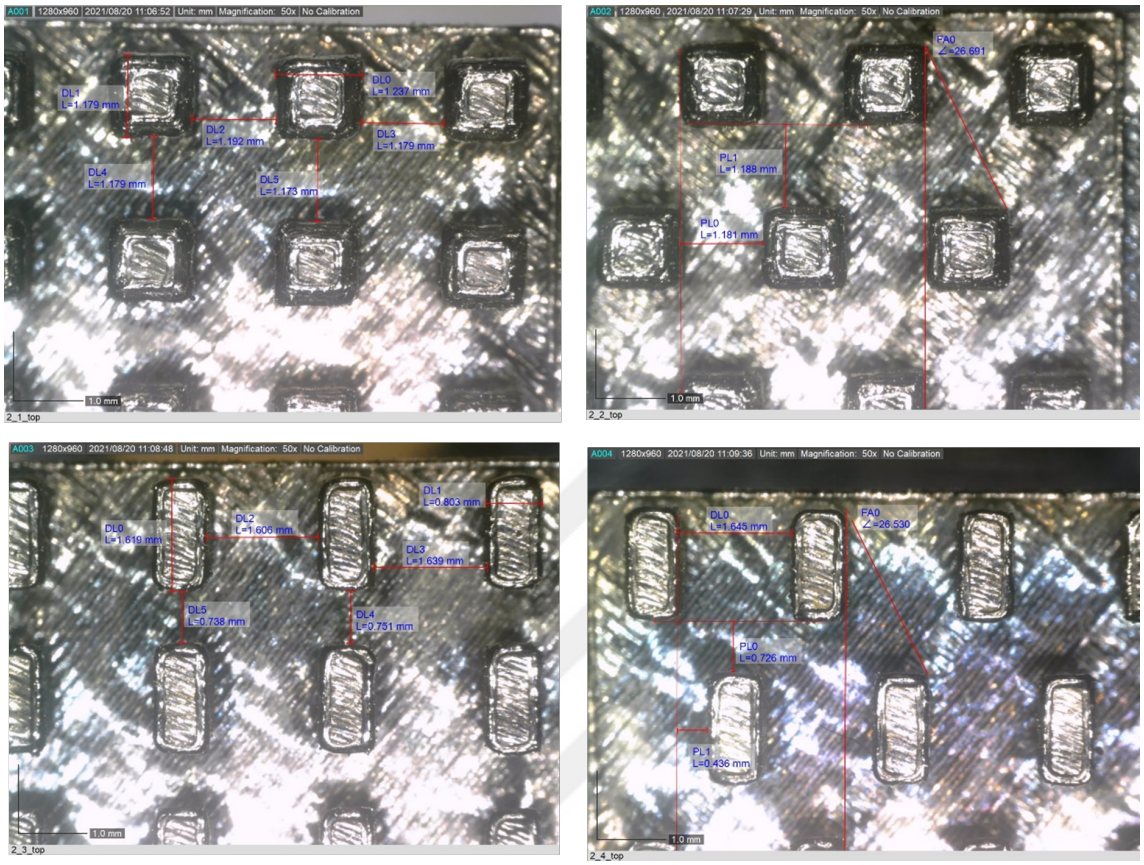

Figure 3.17 Batch 2 - Top view of the four samples

A third batch is manufactured to achieve better polymer infill between the protrusions. Thanks to design freedom provided by additive manufacturing, complex shapes can be designed to aid the infill and consolidation of the polymer during AFP process. For the third batch, various geometries designed are shown in Figures 3.18, 3.19, 3.20 and 3.21. Protrusion height is decreased to 0.6mm for better polymer melt behavior. The experience with the first two batches showed that protrusions density is critical in polymer flow process. Thus, a decreased number of shapes are manufactured in a separated zig-zag pattern as shown in Figure 3.22. Separation between the rows provide the necessary gap to place one layer of tow at 90° which increases the anchoring force of the joint.

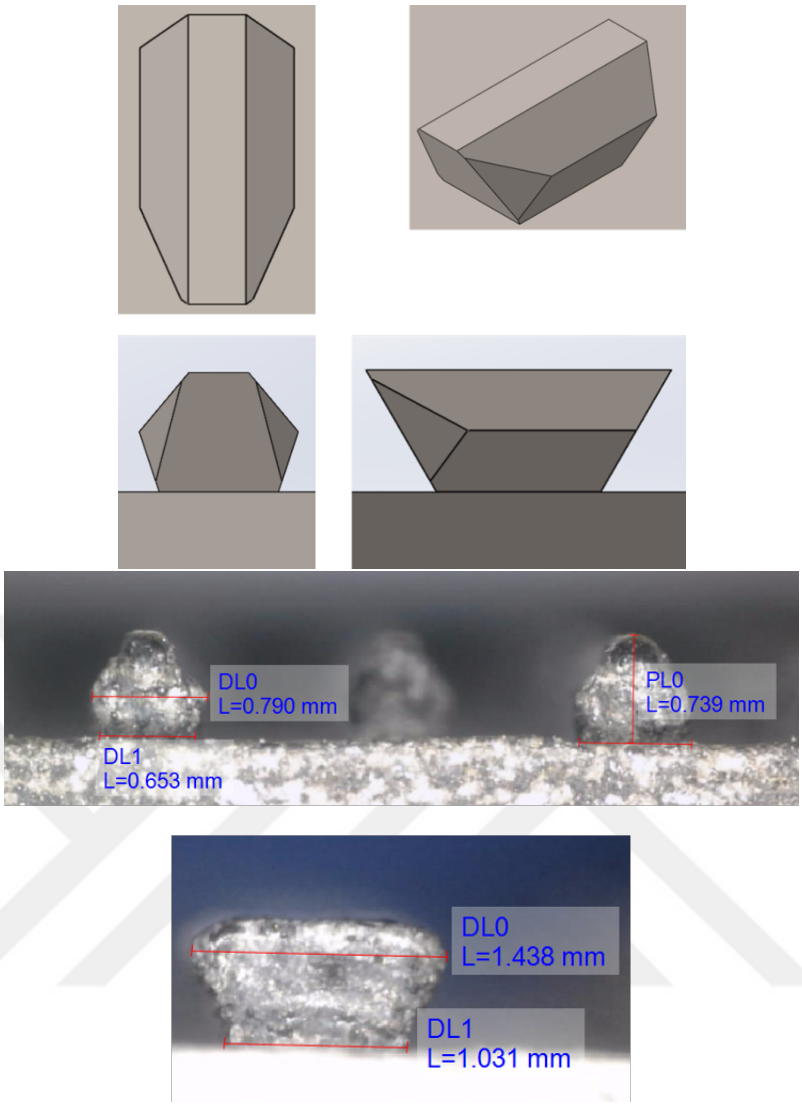

Figure 3.18 Batch 3 - Protrusion shape 1

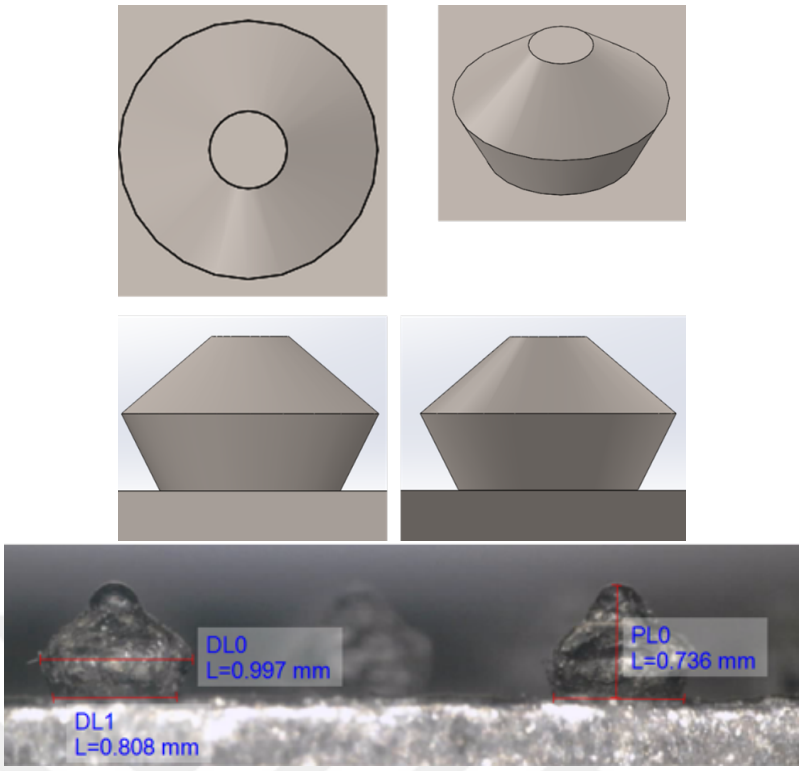

Figure 3.19 Batch 3 - Protrusion shape 2

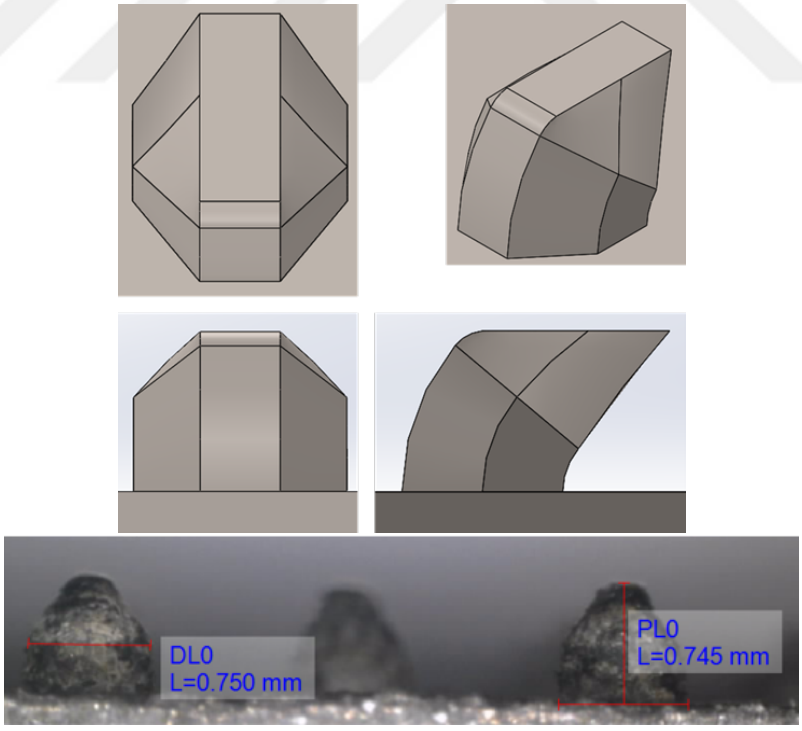

Figure 3.20 Batch 3 - Protrusion shape 3

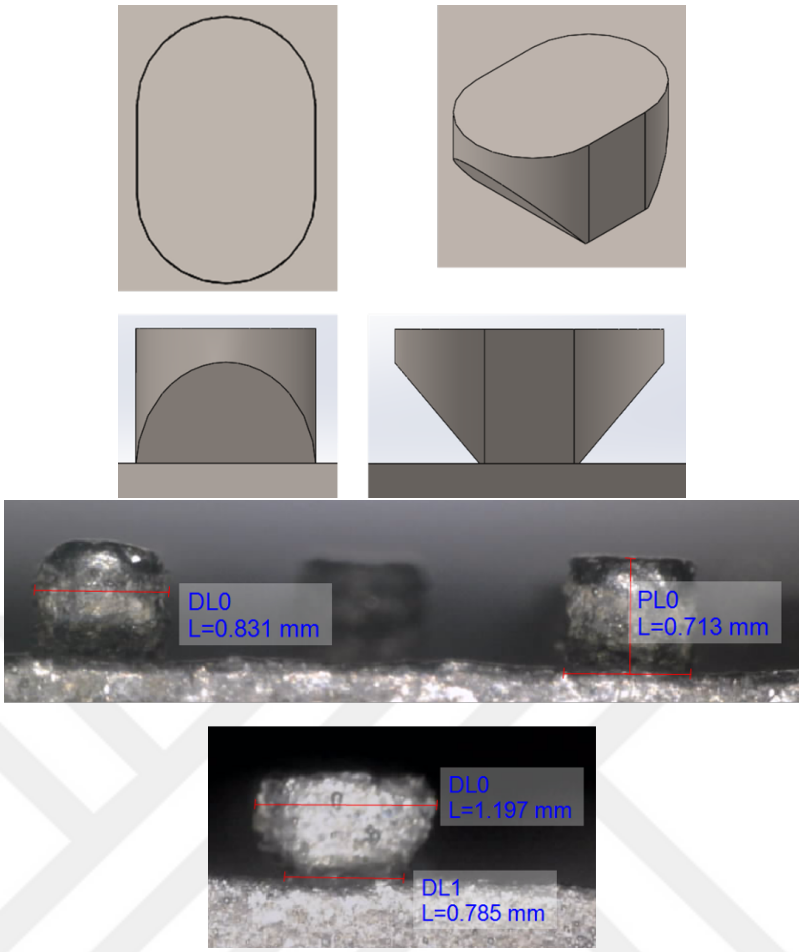

Figure 3.21 Batch 3 - Protrusion shape 4

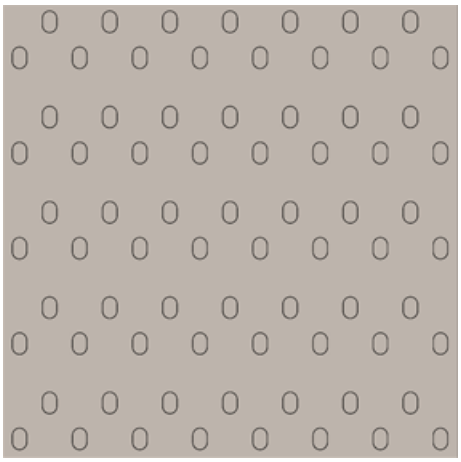

Figure 3.22 Batch 3 - Protrusion placement

3.2.2.2 Heat Treatment

Direct metal laser sintering process creates melt pools by local heating of the laid powder and these melt pools consolidate with previously manufactured layers to form the part, as shown in Figure 3.23. The local application of intense heat causes the material to expand at the vicinity of the radiation while neighboring grids are at much lower temperatures. This phenomenon results in local thermal stresses throughout the part and cannot be avoided. Careful thermal planning and placement of support structures is required to dissipate the heat from the melt zone evenly. Parts may warp after manufacturing using direct metal laser sintering due to high stresses. To avoid deformation of the parts, heat treatment is advised. First

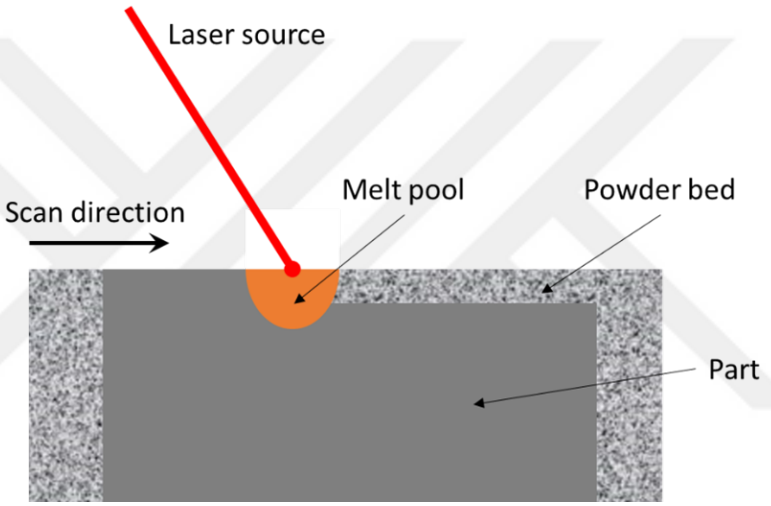

Figure 3.23 DMLS process schematic

two batches of manufacturing for this work have not been heat-treated. As the specimens are wire-cut at the required thickness for lap shear test standard, warping is observed. The amount of warping was acceptable since the specimens were bolted to a fixture during fiber placement, which flattened the specimens during manufacturing. However, the tendency of the metal to recover to its bent shape upon removal from the fixture caused application of strain loads to the bond area. These loads are not quantitatively calculated but they remain a source of decrease in bond strength. At the third batch, the Inconel billet is heat treated at 1065°C for 9 hours in order to accomplish stress relieving and aging. Heat treated batch showed significantly less warping after wire erosion process, as seen in Figure 3.24.

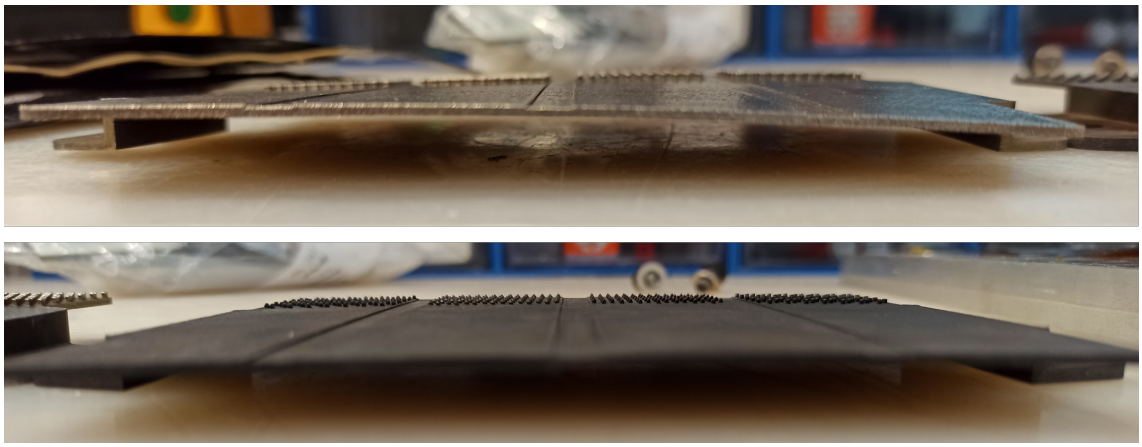

Figure 3.24 As-manufactured sample (top) and heat treated sample (bottom)

3.2.2.3 Surface Properties

Surface topography plays a crucial role in adhesive properties of a part, as discussed in Section 2.2. To evaluate surface properties of the manufactured parts, optical profilometry is used. Surface roughness is evaluated as per ISO 25178 for the area and ISO 4287 for a profile in pulling direction of the lap shear specimens. Measured surface properties are summarized in Tables 3.5 and 3.6. The surface data shows that the maximum adhesion should be achieved in the 3rd batch since it has the highest surface roughness.

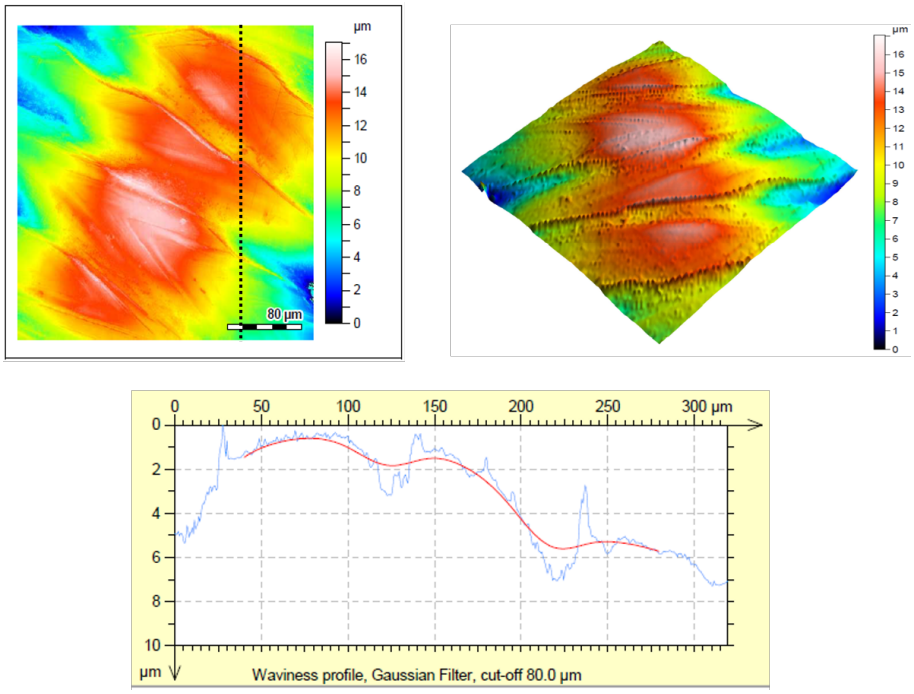

Figure 3.25 Surface topography for Batch 1

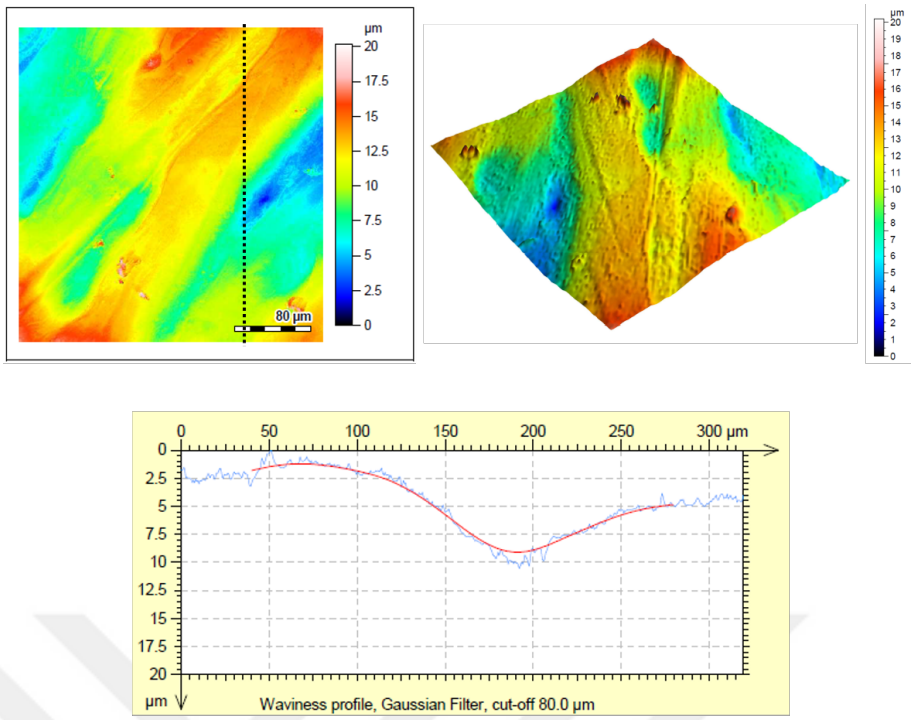

Figure 3.26 Surface topography for Batch 2

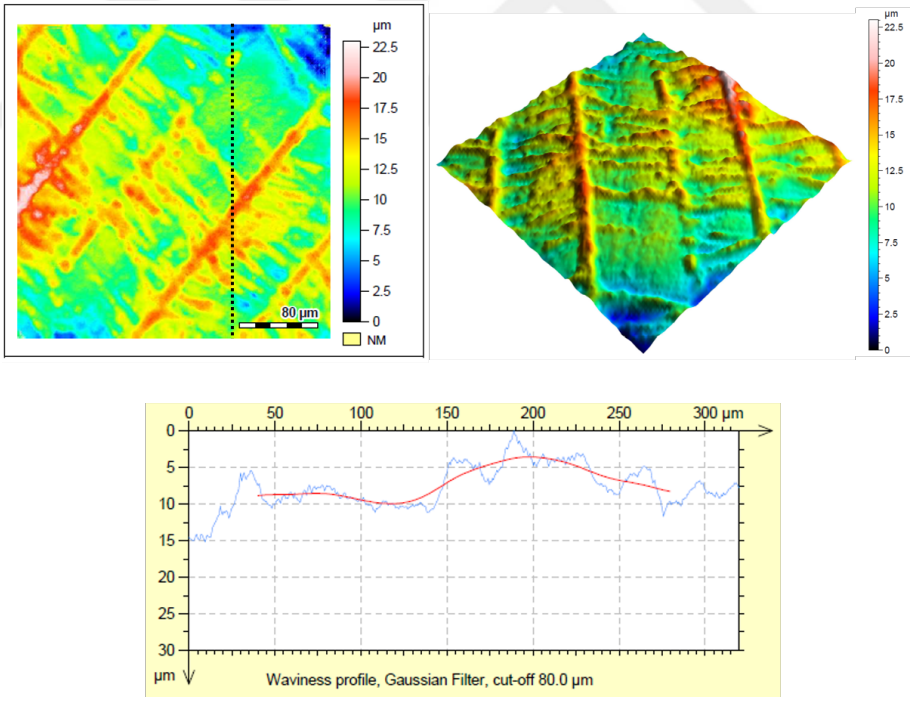

Figure 3.27 Surface topography for Batch 3

Table 3.5 Surface properties as per ISO 4287

Batch Number	ISO 4287 Surface Parameters							
	R_p	R_v	R_z	R_c	R_t	R_a	R_q	R_{sk}
Batch 1	1.45	1.38	2.83	1.82	4.20	0.397	0.550	-0.4
Batch 2	1.09	1.28	2.38	0.948	2.91	0.309	0.420	-0.138
Batch 3	2.66	2.74	5.40	2.50	7.35	1.03	1.23	-0.015

R_p: Maximum profile peak height in μm
R_v: Maximum profile valley depth in μm
R_z: Maximum height of the profile in μm
R_c: Mean height of profile elements in μm
R_t: Total height of the profile in μm
R_a: Arithmetic mean deviation of the profile in μm
R_q: Root mean square deviation of the profile in μm
R_{sk}: Skewness of the profile height distribution

Table 3.6 Surface properties as per ISO 25178

Batch Number	ISO 25178 Surface Parameters						
	S_q	S_p	S_v	S_z	S_a	R_{ku}	S_{sk}
Batch 1	2.98	6.59	10.4	17.0	2.49	2.58	-0.595
Batch 2	2.76	9.88	10.3	20.2	2.30	2.30	-0.178
Batch 3	3.00	11.6	11.4	23.0	23.0	3.24	0.114

S_q: Root mean height of the surface in μm
S_p: Maximum peak height of the surface in μm
S_v: Maximum pit height of the surface in μm
S_z: Maximum height of the surface in μm
S_a: Arithmetical mean height of the profile in μm
S_{ku}: Kurtosis of the surface in μm
S_{sk}: Skewness of the surface

Along with surface topography and roughness measurements, a defining measurement of an adherent surface is the contact angle. Contact angles for the metal specimens are measured with sessile drop tests. A flat-end needle with 243μm inner diameter is used to drop distilled water in room temperature and atmospheric pressure. Droplet shape on the surface is recorded with the integrated camera and built-in circle fitting algorithm of the device software is used to measure contact angles. Measurements are taken from snapshots of the test videos at 10 second intervals until the measured surface angles converge to their static values. 4 tests are conducted on each specimen to average out the irregularities in the manufacturing of

the parts as well as inconsistencies with measurement process. Process is pictured in 3.28 and the results are presented in Table 3.7. Contrary to the surface topography measurements, batch 2 yielded the lowest contact angle and is shown to be the best candidate for good adhesion according to the contact angle measurements.

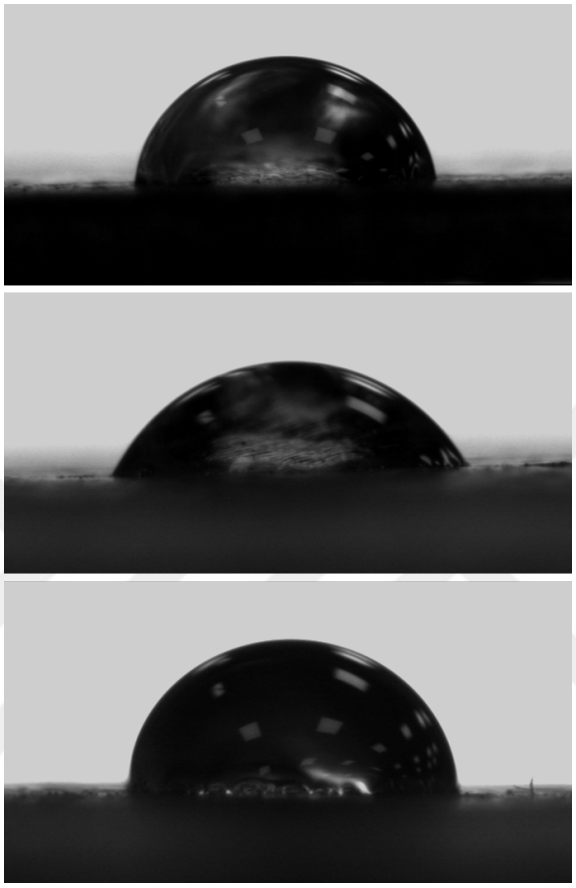

Figure 3.28 Contact angle measurement images for Batch 1 (top), Batch 2 (center) and Batch 3 (bottom)

Table 3.7 Contact angle measurements

Batch Number	Contact Angle Measurements					$1+cos\theta$
	1	2	3	4	Average	
Batch 1	66.0°	70.7°	76.1°	80.3°	73.3°	1.288
Batch 2	61.3°	59.3°	64.3°	55.2°	60.0°	1.500
Batch 3	76.7°	70.6°	80.0°	93.2°	80.1°	1.171

3.2.3 Composite Specimens

Fiber laying process is completed using the Kuka Quantec Robotic AFP cell. AFP is an automated process where pre-impregnated carbon fibers in tape form are heated and set in place via pressure in a single operation. A 6600 W class 4 laser with 650 nm wavelength is used as the heat source which heats the incoming tape as well as the substrate laid previously to initiate interlayer bonding. A compaction roller guides the tapes onto the substrate surface and applies 500 N of compaction force.

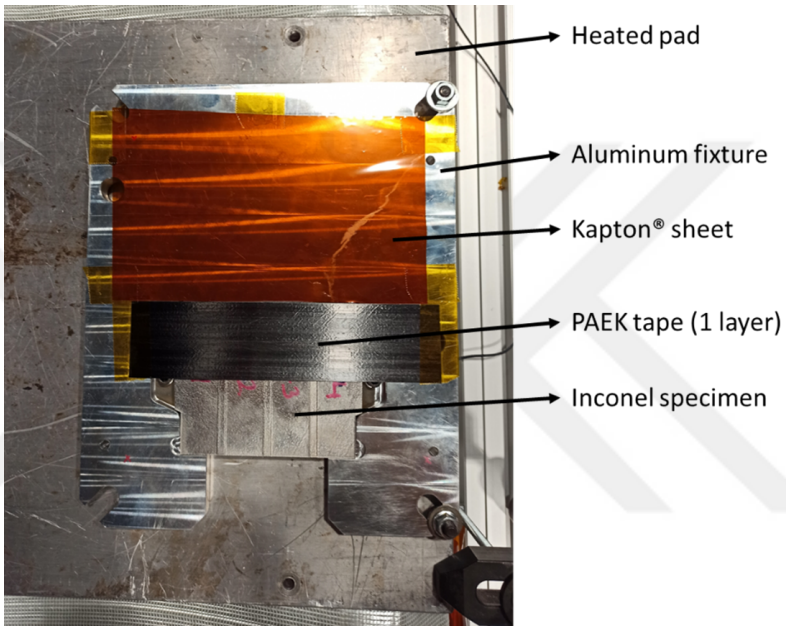

Figure 3.29 Specimen preparation for AFP

The process is valid for thermosets as well as thermoplastics, however thermosets require curing operation after AFP to complete polymerization. Thermoplastic composite parts manufactured via AFP do not require thermal post-processing because polymer entanglement is completed as heat is locally removed from the substrate, allowing crystallization and part consolidation. The cooling rate is crucial in thermoplastic crystallization. The fixture is heated during the process to aid consolidation of the thermoplastic resin. To avoid laser scattering off the Aluminum fixture during the first layer of fiber placement and possible damage to the equipment, Kapton® sheet is applied onto the flat surface before the AFP process. Protrusions are covered with a single layer of PAEK tape for the same reason. In later iterations, the protrusions are covered with 2 layers of PEEK film, instead of carbon fiber reinforced PAEK tape which prevented complete filling of the space between the protrusions.

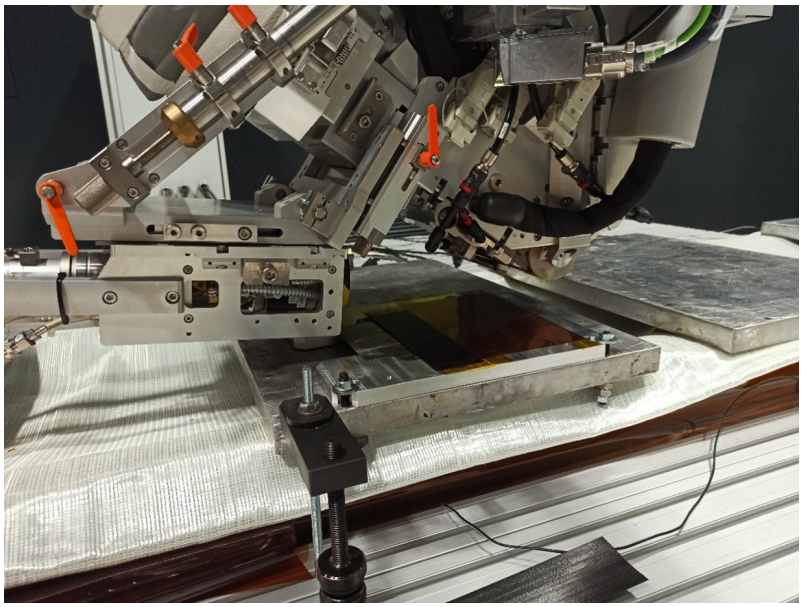

Figure 3.30 AFP setup

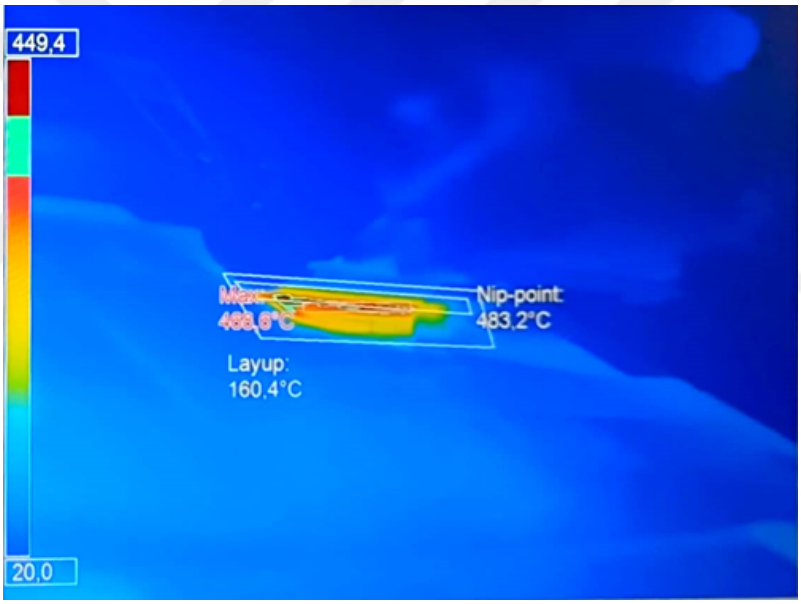

Figure 3.31 Thermal view of AFP process

The specimens are manufactured with a low fiber layup speed of 50mm/s to enhance thermoplastic flow in between the protrusions. 500 N compaction force is applied by the roller onto the laid tapes to aid with stiction to previous layers. Thermal imaging of the process as seen in Figure 3.31 revealed that temperatures higher than 400°C is reached at the nip point. In average, the temperature of the tapes during consolidation is around 400°C, as seen on the thermal history of AFP process in Figure 3.32. The surface temperature of the previously laid tapes, named as layup, is between 160°C and 200°C during AFP.

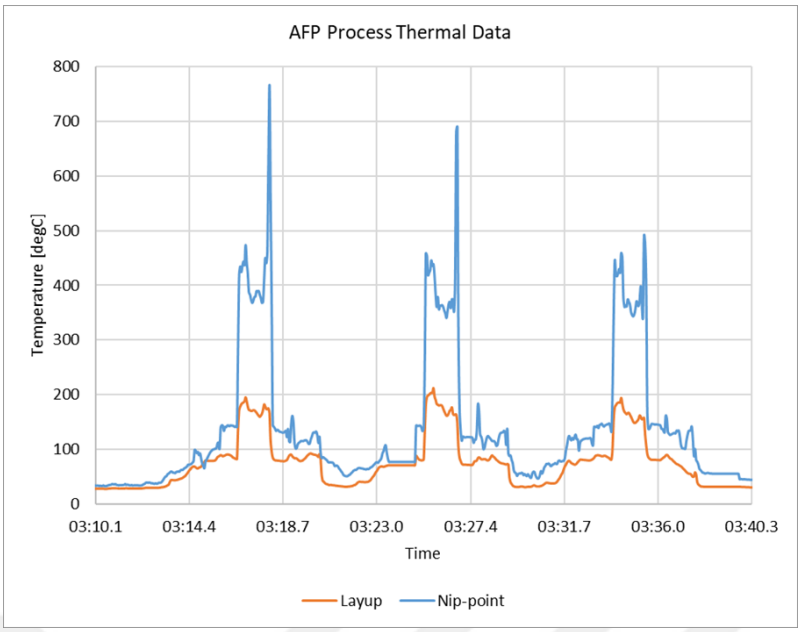

Figure 3.32 AFP thermal history

3.3 Testing

A robust way of creating hybrid joints is to use double-lap configuration. However, additive manufacturing of the part with protrusions on both sides for double lap shear test would require special attention in support generation and thermal management in comparison to a single-sided metal specimen utilized in this work. Also, AFP on such a specimen would require special considerations such as a mandrel or rotating fixture. Another test often run for adhesive evaluation is the peel test ASME D 1876. Again, manufacturing metal specimens as required by peel test standard would require higher machine times and extra difficulties in post processing. AFP operation on these specimens would also require a different set of special fixturing. Thus, the feasible single-lap shear test is chosen.
Conventionally, single lap shear tests are suitable for assemblies where the bond strength of adhesively joined specimens is evaluated. In most cases, adhesively joined parts are loaded in shear, therefore this test is a good representation in evaluation of adhesive performance. Single lap shear test as per ASTM-D-5868 are conducted to evaluate the hybrid bond strength of the additively manufactured specimens of this work, with test layout presented in Figure 3.33. The specimens are connected to Instron 5982 axial test bench with a 4-inch grip separation. The loading rate is 0.5 in./min (13 mm/min).

Besides the simplicity of single lap shear testing, some complications as evaluated

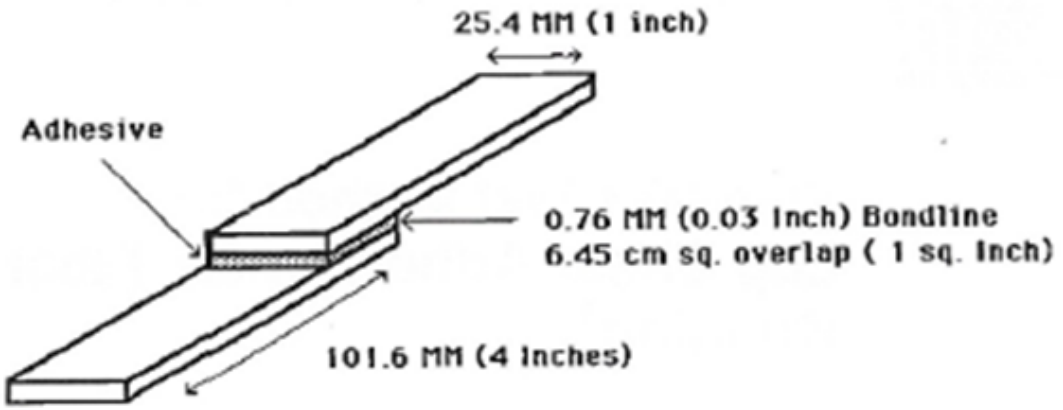

Figure 3.33 Single lap shear test specimen ASTM

by Redmann et al. are inherently present (Redmann et al., 2021). First problem is the uneven stress distribution within the adhesive layer, as demonstrated in Figure 3.34. Under low loads, the adhesive zone is under minimal strain and no elongation is detected (top). At intermediate loads, the adhesive zone elongation and shear stress distribution within the adhesive is even (center). At high loads, the elongation of the adhesive and shear stresses are higher at the edges of the bond line (bottom). This is a result of the uneven tensile stress throughout the bond length and therefore progressively decreasing tensile strains, resulting in a distorted deformation of the adhesive. In the hybrid joint in this work, these issues are amplified due to discontinuity of material at the bond-line.

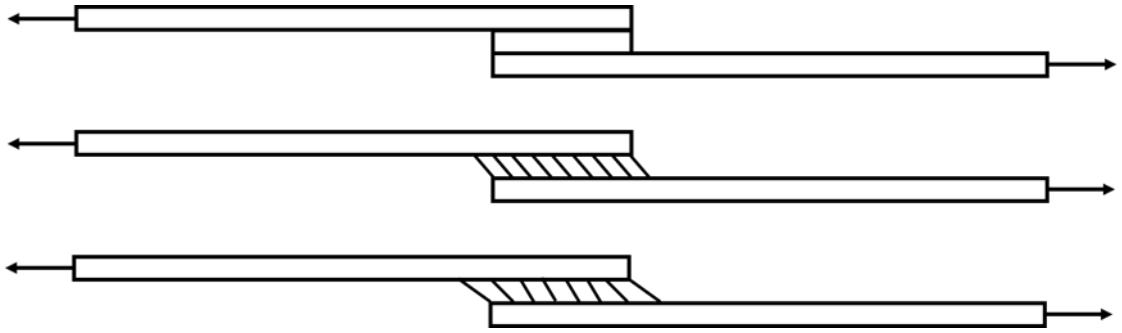

Figure 3.34 Single lap shear adhesive elongation – redrawn from Redmann et al.

Another problem that comes with the simplicity of the test is the eccentricity in the load path. As the specimen is pulled at its edges, the line of loading connecting the grippers is as the dashed red line seen in Figure 3.35. This oblique force prevents the adhesive to be loaded by pure shear and bending occurs at the joint location. In fact, almost all failures at tensile loading of such specimens are due to peeling of the adhesive, rather than shear. To avoid this, several tabs are manufactured from available scrap materials and the test geometry is changed to the configuration in Figure 3.36.

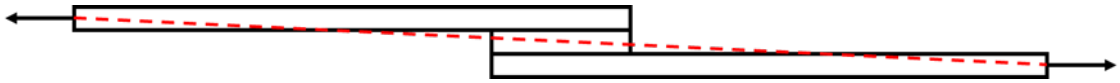

Figure 3.35 Load eccentricity in single lap shear testing – redrawn from Redmann et al.

Figure 3.36 Eccentricity correction using tabs (yellow)

3.3.1 Test Plan

A total of 12 specimens have been manufactured in three batches. 4 of these are the failed parts at the DMLS due to too small feature sizes (Batch 1). These specimens are used for process refinement purposes for AFP, water jet cutting and lap shear testing. The test plan is presented in Table 3.8.

Table 3.8 Single lap shear test plan

Batch Number	Specimen Number	Test Name
Batch1	1-1	Test 1-1
	1-2	Test 1-2
	1-3	Test 1-3
	1-4	Test 1-4
Batch2	2-1	Test 2-1
	2-2	Test 2-2
	2-3	Test 2-3
	2-4	Test 2-4
Batch3	3-1	Test 3-1
	3-2	Test 3-2
	3-3	Test 3-3
	3-4	Test 3-4

4. LABORATORY EQUIPMENT

In this section, the equipment that is used during this thesis is presented. Each machine has its own operating and programming interface, as well as special considerations for smooth operation. Therefore, the expertise of the specialists/operators has been crucial in enabling the work presented in this thesis to be completed.

4.1 EOS M290 Direct Metal Laser Sintering Machine

Metal additive manufacturing machine used to manufacture samples is EOS M290 Direct Metal Laser Sintering (DMLS) Machine. This equipment offers a build volume of 250 x 250 x 325 mm and is equipped with a Yb-fiber laser rated at 400 W. The focus diameter of the laser is advertised at 100 μm but as a rule of thumb, feature sizes are limited to 300 μm minimum for precise manufacturing. A wide selection of materials such as aluminum, steel titanium and nickel alloys can be manufactured by M290. SUIMC has abundance of Nickel alloys (Inconel) that are used in high temperature regions of several jet engines. Metal specimens for the scope of this thesis are therefore manufactured in Inconel 718. The machine is shown in Figure 4.1.

Figure 4.1 EOS M290 DMLS printer

4.2 Nabertherm Heat Treatment Furnace

A Nabertherm N41/H heat treatment furnace is used on the Inconel parts after manufacturing as a stress relief operation. The furnace is capable of sustaining up to 1280°C temperature for parts up to dimensions 350 x 500 x 250 mm.

Figure 4.2 Nabertherm heat treatment furnace

4.3 Mitsubishi FA20S Wire EDM Machine

Removal of the Inconel parts from the buildplate is done in single step via wire EDM for precision machining as opposed to using a bandsaw and milling to required dimensions. A Mitsubishi FA20S machine shown in Figure 4.3 is used at ARK Kalıp company in Istanbul. The machine movement capability is 500, 350 and 300 mm stroke in x, y and z directions respectively. The machine can cut a workpiece of maximum 1500 kg with 1050 x 800 x 295 mm dimensions. A wire electrode with 0.25 mm diameter is used.

Figure 4.3 Mitsubishi FA20S wire EDM machine

4.4 Dino-Lite AD7013MZT Microscope

To measure the additively manufactured protrusions in 3 dimensions, a portable microscope solution was required because the workpiece is larger than the z-movement capabilities of standard desktop optical microscopes. Thus, a Dino-lite microscope with up to 200x magnification and integrated LED lighting is used.

Figure 4.4 Dino optical microscope

4.5 Nano Focus μsurf Non-Contact 3D Profilometer

To define the surface topography of additively manufactured Inconel parts, a non-contact optical profilometer is used. An 50x optical lens is used to capture the surface texture with as much detail as possible. Captured surface data is analyzed using μsoft analysis software.

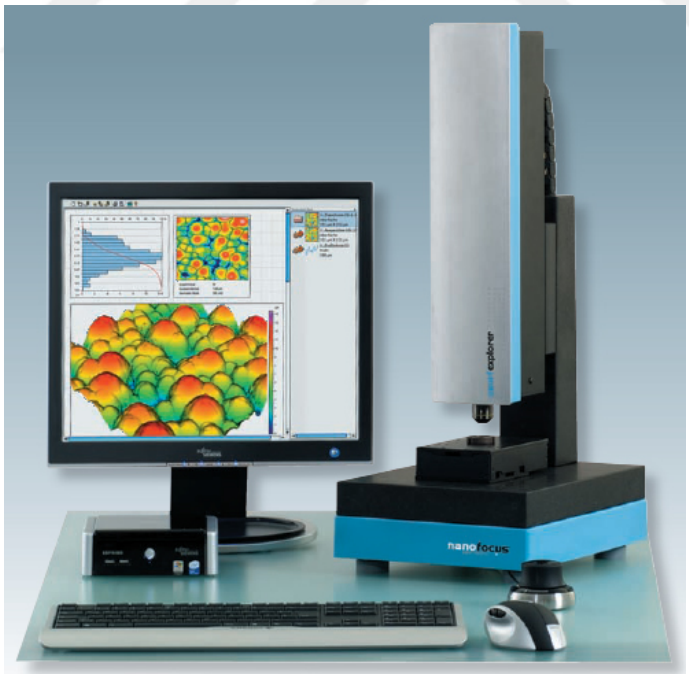

Figure 4.5 Nano Focus μSurf non-contact 3D profilometer

4.6 KRÜSS DSA 10 Mk2 Drop Shape Analyzer

Contact angles for metallic parts manufactured via selective laser melting are analyzed conducting sessile drop tests on a Krüss drop shape analyzer. The integrated camera is capable of capturing images with 80ms intervals for dynamic measurements.

Figure 4.6 KRÜSS DSA 10 Mk2 drop shape analyzer

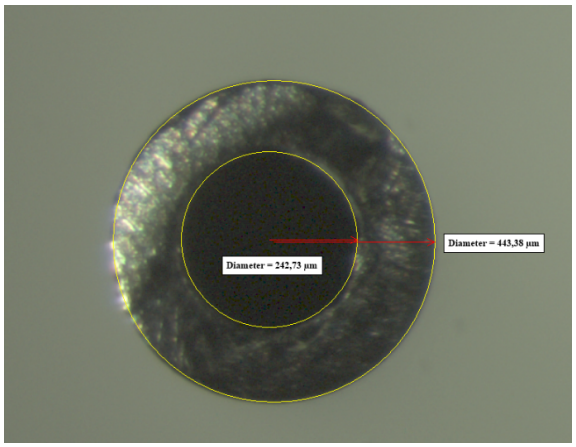

Figure 4.7 Needle tip used for sessile drop tests

4.7 Coriolis C2 Robotic Automated Fiber Placement (AFP) Cell

The composite manufacturing for the test specimens is done in the Coriolis C2 robotic AFP cell in advanced composites lab at SU IMC. The robot is KUKA Quantec KR210 R3100 moving on Güdel 8-meter linear axis. This cell can manufacture on molds up to 6 meters length, and the mandrel allows manufacturing on cylindrical molds up to 3meters in diameter (Sabancı University Integrated Manufacturing Center, 2021). The end effector of the robot is capable of laying down 8 tows at a time, corresponding to 2 inches in width.

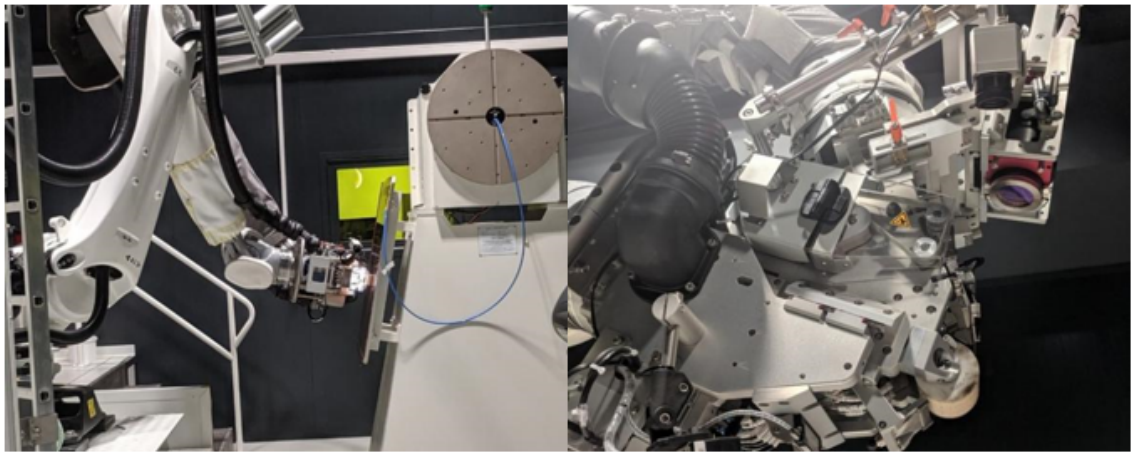

Figure 4.8 Robotic AFP cell

4.8 Robotic Abrasive Water Jetting (AWJ) Cell

SU IMC Unconventional and Robotic Manufacturing facilitiy hosts a robotic AWJ cell that is used to cut single test specimens out of batches of four manufactured via AFP. The KUKA KR16 ULTRA-F over hanged robot that is mounted on a 3-meter rail allows part manufacturing on a 2.5 m x 2.5 m work table. A KMT waterjet pump rated at 3800 bar provides a high pressure abrasive-water mix through a nozzle for precision cutting of the specimens.

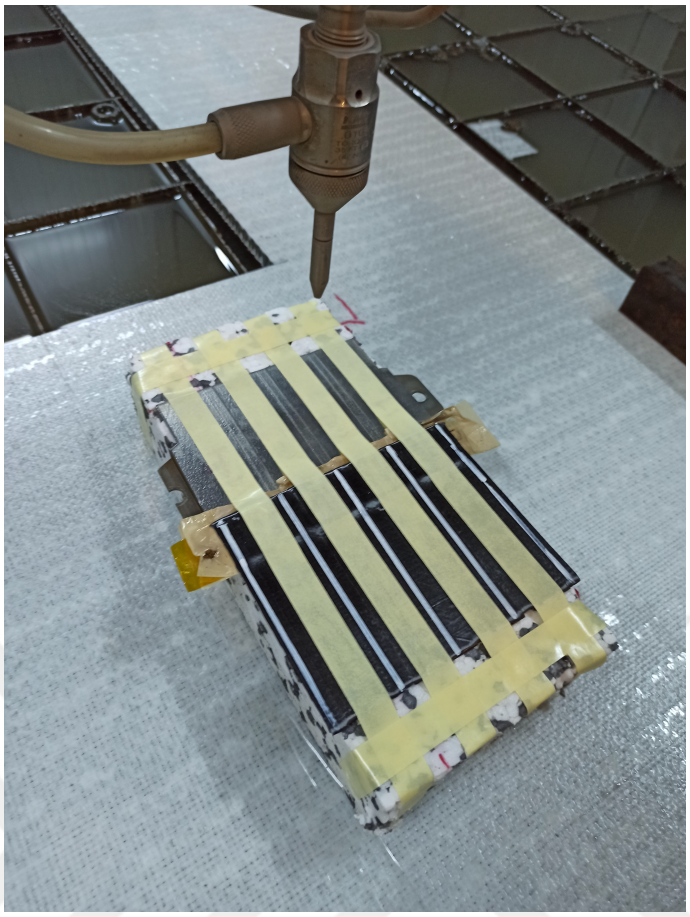

Figure 4.9 Specimen preparation in abrasive water jet cell

4.9 Instron 5982 Universal Electromechanical Test Machine

Single lap shear tests are conducted in Mechanical Test Laboratory of SU IMC on Instron 5982 test machine. The equipment is capable of 100 kN axial loading up to 1016 mm/min separation speed. The built-in strain measurement apparatus consists of an extensometer with 25mm gauge-length, a quarter-bridge strain gauge with 4 channels at 120 ohms.

Figure 4.10 Instron 100kN electromechanical test machine

5. TESTS & RESULTS

5.1 Lap Shear Tests

To allow a direct comparison to adhesive joints, the bond area is treated as homogeneous in test evaluation. It should be noted that shear and stress values within the bond geometry locally exceeds the averaged values presented here.

Table 5.1 Single lap shear test results

Batch Number	Specimen Number	Results		
		Maximum Load [N]	Maximum Avg. Shear Stress [MPa]	Shear Modulus [MPa]
Batch1	1-1	5473.32	7.76	23.92
	1-2	4097.16	5.55	21.73
	1-3	3121.91	4.32	20.05
	1-4	4058.43	5.57	19.53
Batch2	2-1	870.39	1.30	9.61
	2-2	597.80	0.89	9.71
	2-3	1718.27	2.56	7.48
	2-4	1886.96	2.81	15.99
Batch3	3-1	9.61	0.01	0.07
	3-2	323.47	0.46	3.97
	3-3	1443.52	2.10	3.04
	3-4	1484.61	2.15	6.96

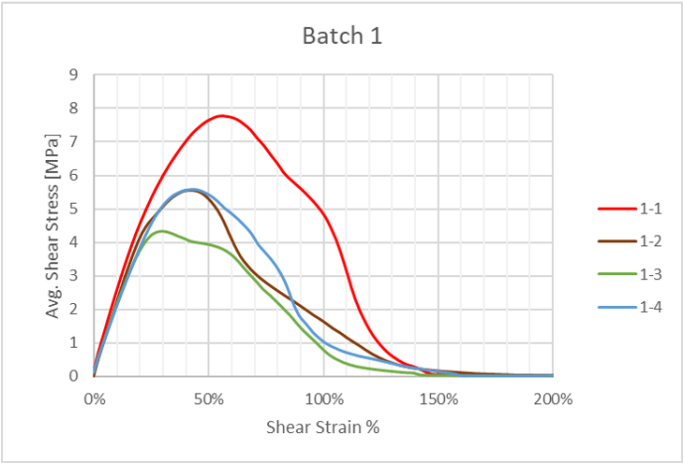

Figure 5.1 Shear response of hybrid bond, Batch 1

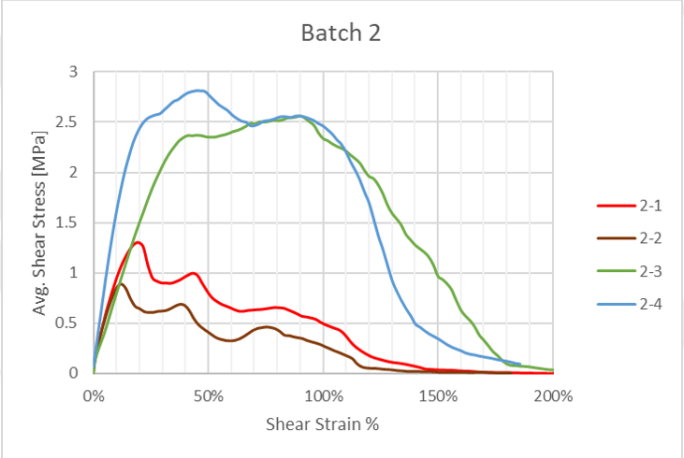

Figure 5.2 Shear response of hybrid bond, Batch 2

Figure 5.3 Shear response of hybrid bond, Batch 3

5.2 Infill Evaluation

To assess the success of infill between the protrusions after AFP and failure modes of the joints after shear testing, the cross-sections of the specimens are obtained for inspection. As shown in Figure 5.4, thermoplastic resin was not able to fill the gaps sufficiently. Diagonal placement of the protrusions demonstrated better infill overall. No yielding is observed in the metal protrusions and expected tear-out is not present in composite specimens. Failure of the joints are observed to occur in pull-out direction which indicates insufficient anchoring between the two parts.

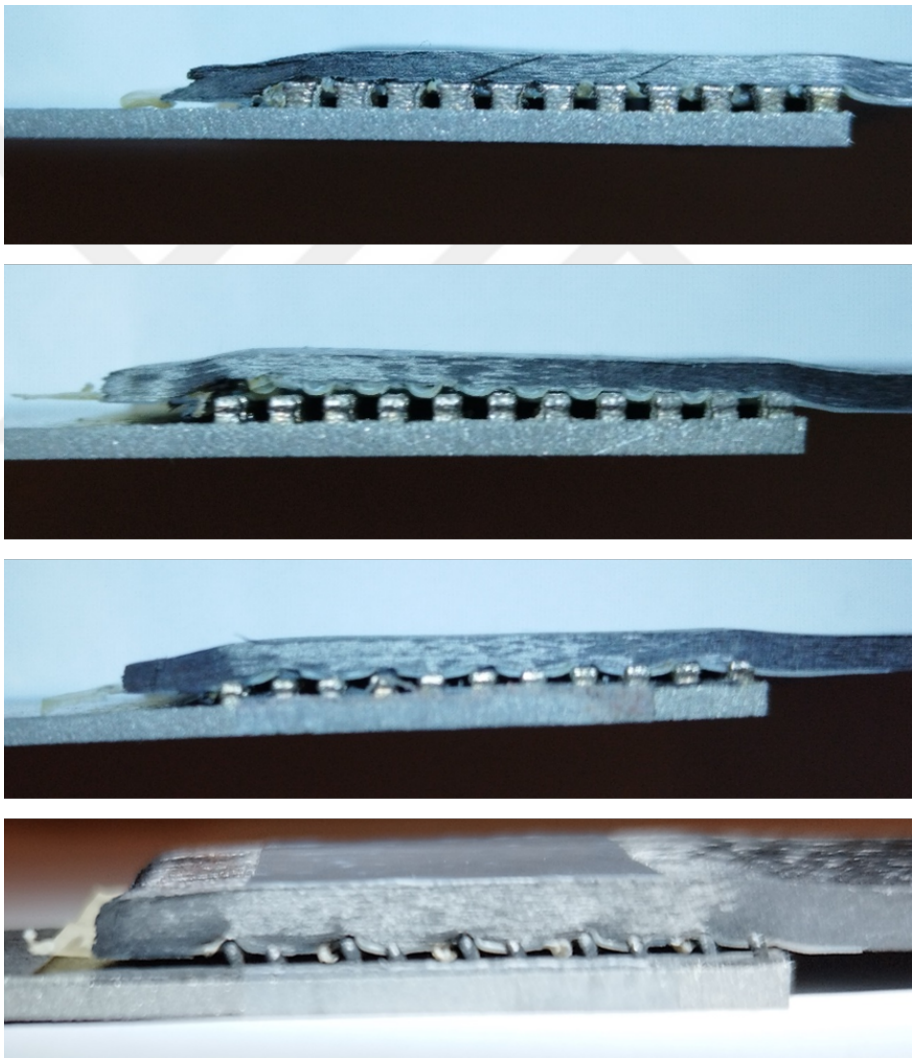

Figure 5.4 Cross-section view of joints after failure

5.3 Second Test Campaign

It has been deduced that the AFP process parameters were not optimized for successful infill between the protrusions due to limitations regarding the safe operation of the machinery. To evaluate the achievable strength values for a more successful infill, a second round of testing is conducted. Using the same metal specimens and consolidated thermoplastic parts, joints with better infill have been manufactured with the help of a hot press. This process is more parallel to the existing overmolding method for thermoplastic to metal joining and not within the scope of this thesis, however it was beneficial to conduct as a proof-of-concept study.

The parts were pressed together in a manual hot press at a temperature of 260°C. A clamping force of 2000 N is applied onto the batches that consist of 4 test specimens. The parts are allowed to cool down to ambient temperature overnight, no cooling is applied. Test specimens manufactured via the hot press are shown in Figure 5.5.

Figure 5.5 Test specimens re-joined with hot press

Table 5.2 Second test campaign results

Batch Number	Specimen Number	Results		
		Maximum Load [N]	Maximum Avg. Shear Stress [MPa]	Shear Modulus [MPa]
Batch1	1-2	4114.60	6.53	27.61
	1-3	1824.10	2.89	23.67
	1-4	4228.19	6.89	28.00
Batch2	2-2	8993.47	13.58	35.22
	2-3	4862.31	7.49	37.65
	2-4	12562.62	19.24	35.79
Batch3	3-2	1447.47	2.14	13.97
	3-3	529.58	0.80	5.57
	3-4	4262.97	6.31	19.65

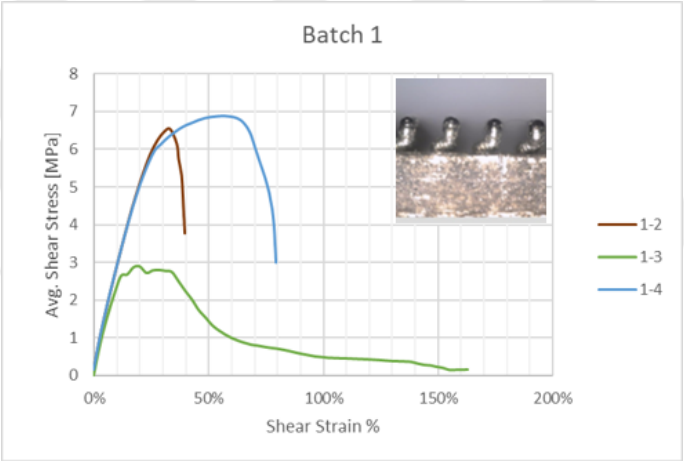

Figure 5.6 Shear response of re-joined hybrid bond, Batch 1

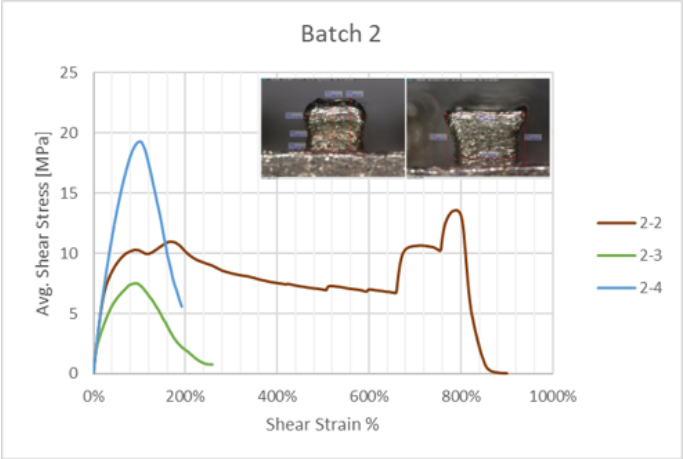

Figure 5.7 Shear response of re-joined hybrid bond, Batch 2

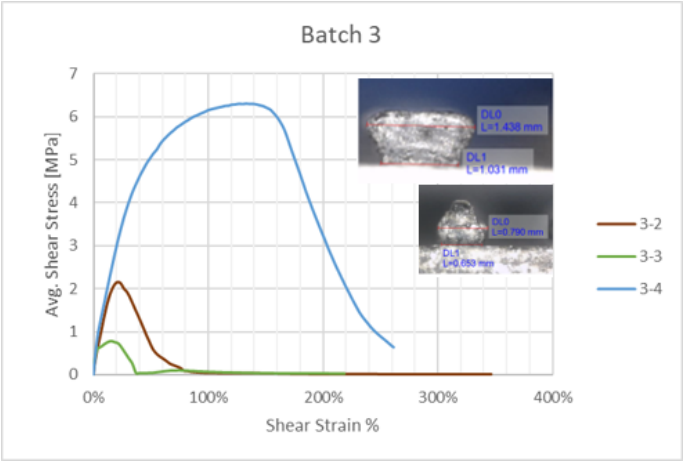

Figure 5.8 Shear response of re-joined hybrid bond, Batch 3

Test results for the second campaign have high standard deviation, however several positive aspects have been observed. The first and most important one is the achievement of better infill between the protrusions. This is evident by the shear-out failure of the specimens instead of pull-out failure observed previously, as shown in Figure 5.9. Strength values comparable with adhesive joining are obtained in the second test campaign.

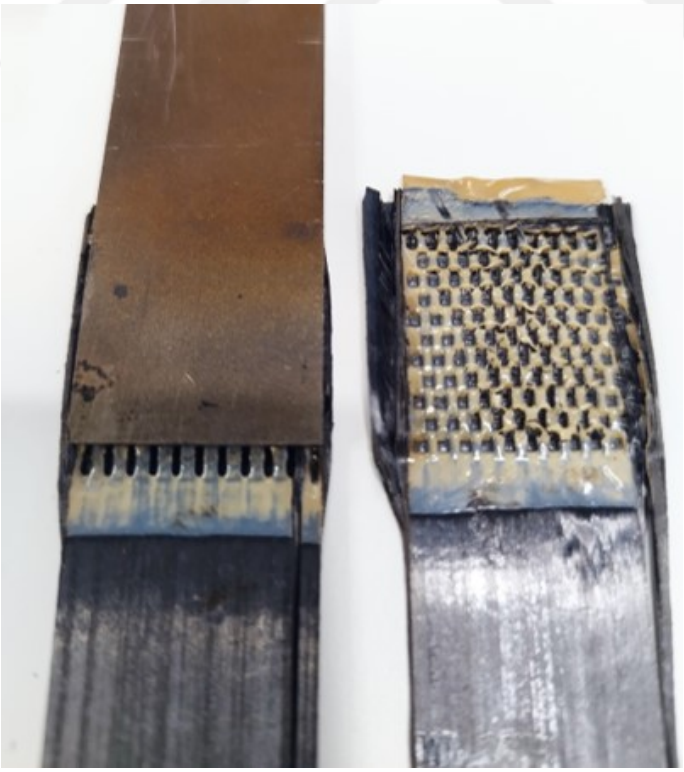

Figure 5.9 Shear-out and pull-out failures

6. CONCLUSION

In this thesis work, the feasibility of in-situ hybrid bond creation between additively manufactured metals with special surface protrusions and thermoplastic-carbon fiber composites using automated fiber placement method is investigated.

The proposed method of creating hybrid joints via thermoplastic AFP has yielded comparable strength values to some of the special joints for thermoplastics in literature. The closest method to this work is the use of overmolding in U-joining (Feistauer & Amancio-Filho, 2018). The presented method in this thesis is promising in the way that lap shear test results, despite the imperfect bonding, demonstrate comparable strength. In comparison with the adhesive joints, the lack of process optimization with AFP method caused lesser strength.

There are several issues that inhibited a perfect end result. First setback is the evident low stiction between thermoplastic and inconel. For all batches, AFP process with conventional mold temperature of 180°C failed to constitute sufficient polymer flow between the protrusions. In spite of geometrical efforts to achieve interlocking, the manufactured specimens were unable to demonstrate meaningful strength in pullout direction. Nonetheless, the bond strength in shear direction, evident by the high shear moduli of the joints before failure, are promising. Therefore, this method can be used with higher success in cylindrical geometries such as actuators, shock absorbers or bearings that are to be installed inside/between composite parts, by winding the thermoplastic composite around the axis using a mandrel.

Process parameters were manipulated until the capabilities of the manufacturing equipment were reached. Mold temperatures during AFP are increased up to 230°C to help with polymer flow. Other helpful parameters for the AFP process are the layup speed and compaction force. Layup speed was decreased down to 4mm/sec, however the compaction force could not be increased higher than 500N due to safety concerns.

Better polymer and fiber flow between the protrusions could have been achieved with the help of a special compaction roller. The standard roller is an elastic cylindrical

tool that is coated with a special layer to accommodate high process temperatures and pressures without the polymer sticking to the roller. The special roller would incorporate smaller features that can penetrate between the protrusions to force a higher flow. However, it is not feasible to manipulate the equipment for each protrusion geometry and spacing.

One aim of the project was to evaluate the effects of surface topography in joint strength. Conventionally, higher surface roughness and lower contact angle specimens were expected to create bonds with higher strength. However, high standard deviation within the test results and lack of intimate contact between the parts prevented deduction of a meaningful relationship between the surface properties and bond strength.

The second test campaign revealed that the proposed method is capable of manufacturing joints with high strength. Strength values up to 19.24 MPa were achieved when the infill between the protrusions were better managed. This result is very promising even compared to adhesive joints. It should also be noted that the composite parts, due to smaller size of the fixture, were manufactured unidirectionally, and the fibers were oriented in parallel to the load applied. This resulted in shearing of the matrix of the composite and the fibers were not able to contribute to the joint strength to the required level. Conventionally, parts in production are not unidirectional and intertwining of the fibers in different orientations would increase the anchoring force around the protrusions.

The novelty of presented work is in creation of the joints in-situ by means of co-consolidation. A major advantage of the presented method of manufacturing hybrid bonds is the ability to create required assembly with maximum automatization. No special secondary tooling is required once the process is defined. Robotic and additive manufacturing allows the manufacture of parts that can directly be used without extra machining or assembly operations. Another strength of the method is the lack of fasteners and weight saving on the assembled parts. A major concern for and industrial process is the cost and additive manufacturing processes currently are more expensive methods of producing parts. However, the flexibility and automatization provided by using additive manufacturing processes will decrease the amount of "scrapped" parts, which are unfortunate byproducts of using manual labor to join dissimilar materials with conventional techniques. On top of decreasing the amount of material and time waste, this method is applicable on a scale. Additive manufacturing technologies such as direct energy deposition (DED) offer the chance to manufacture with precision the proposed surface protrusions onto larger metal parts that are conventionally machined, and AFP, being a robotic process, is capable of

manufacturing the composite interfaces along with the parts themselves.

This thesis work demonstrated that in-situ co-consolidation of thermoplastics and additively manufactured metals to form hybrid bonds is possible, feasible and yields good strength. With optimization of the AFP process for the specific joint geometries, the proposed method for joining dissimilar materials for aerospace and automotive structural applications may yield considerable advantages over the conventional joining methods.

REFERENCES

Abdel Wahab, M. (2012). Fatigue in adhesively bonded joints: A review. *ISRN Materials Science*, *2012*.

Abulizi, D., Duan, Y., Li, D., & Lu, B. (2011). A new method for glass-fiber reinforced composites manufacturing: Automated fiber placement with in-situ uv curing. In *2011 IEEE International Symposium on Assembly and Manufacturing (ISAM)*, (pp. 1–4).

Amancio-Filho, S., Bueno, C., dos Santos, J., Huber, N., & Hage, E. (2011). On the feasibility of friction spot joining in magnesium/fiber-reinforced polymer composite hybrid structures. *Materials Science and Engineering: A*, *528*(10), 3841–3848.

Amancio-Filho, S. T., Feistauer, E. E., & dos Santos, J. (European Patent No. EP 3 078 480 A1, 2015). Method for connecting a surface-structured workpiece and a plastic workpiece.

Amend, P., Hentschel, O., Scheitler, C., Gorunov, A. I., & Schmidt, M. (2015). Effect of additive manufactured metallic structures on laser-based thermal joining of thermoplastic metal hybrids. In *Material Forming ESAFORM 2015*, volume 651 of *Key Engineering Materials*, (pp. 777–782). Trans Tech Publications Ltd.

Amend, P., Pfindel, S., & Schmidt, M. (2013). Thermal joining of thermoplastic metal hybrids by means of mono- and polychromatic radiation. *Physics Procedia*, *41*, 98–105. Lasers in Manufacturing (LiM 2013).

ASTM. *ASTM-D-5868 Standard Test Method for Lap Shear Adhesion for Fiber Reinforced Plastic (FRP) Bonding*.

Barbarisi, M. (1967). Relationship between wettability and adhesion of polyethylene. *Nature*, *215*, 383–384.

Beraud, N., Vignat, F., Villeneuve, F., & Dendievel, R. (2014). New Trajectories in Electron Beam Melting Manufacturing to Reduce Curling Effect. In *CIRP CMS 2014*, volume 17, (pp. 738–743)., Windsor, Canada.

Bianchi, F. (2012). *Numerical modelling of through-thickness reinforced structural joints*. PhD thesis, Cranfield University.

Boschetto, A. & Bottini, L. (2016). Design for manufacturing of surfaces to improve accuracy in fused deposition modeling. *Robot. Comput.-Integr. Manuf.*, *37*(C), 103–114.

Brasington, A., Sacco, C., Halbritter, J., Wehbe, R., & Harik, R. (2021). Automated fiber placement: A review of history, current technologies, and future paths forward. *Composites Part C: Open Access*, *6*, 100–182.

Dorey, G. (1987). Carbon fibres and their applications. *Journal of Physics D: Applied Physics*, *20*(3), 245–256.

Dutta, B. & Froes, F. H. (2016). Chapter 4 - microstructure and mechanical properties. In B. Dutta & F. H. Froes (Eds.), *Additive Manufacturing of Titanium Alloys* (pp. 41–50). Butterworth-Heinemann.

Ebel, T., Amancio-Filho, S. T., & dos Santos, J. (European Patent No. EP 2 468 436 B1, 2013). Method for manufacturing metal casings with structured surfaces.

Feistauer, E. E. & Amancio-Filho, S. T. (2018). Ultrasonic joining of lightweight alloy/fiber-reinforced polymer hybrid structures. In Amancio-Filho, S. T. &

Blaga, L.-A. (Eds.), *Joining of Polymer-Metal Hybrid Structures*, (pp. 307–333). John Wiley & Sons, Ltd.

Fera, M., Fruggiero, F., Lambiase, A., & Macchiaroli, R. (2016). State of the art of additive manufacturing: Review for tolerances, mechanical resistance and production costs. *Cogent Engineering*, *3*.

G. Pérez-de Eulate, N., Iztueta, A. A., Gondra, K., & Vallejo, F. J. (2020). Influence of the fibre content, exposure time, and compaction pressure on the mechanical properties of ultraviolet-cured composites. *Journal of Composites Science*, *4*(1).

Han, X., Crocombe, A., Anwar, R., Hu, P., & Li, W. (2014). The effect of a hot–wet environment on adhesively bonded joints under a sustained load. *Journal of Adhesion*, *90*.

Kohl, M.-L., Schricker, K., Bergmann, J. P., Lohse, M., Hertel, M., & Füssel, U. (2018). Thermal joining of thermoplastics to metals: Surface preparation of steel based on laser radiation and tungsten inert gas arc process. *Procedia CIRP*, *74*, 500–505. 10th CIRP Conference on Photonic Technologies [LANE 2018].

Lambiase, F., Scipioni, S. I., Lee, C.-J., Ko, D.-C., & Liu, F. (2021). A state-of-the-art review on advanced joining processes for metal-composite and metal-polymer hybrid structures. *Materials*, *14*(8).

Lewandowski, J. & Seifi, M. (2016). Metal additive manufacturing: A review of mechanical properties. *Annual Review of Materials Research*, *46*, 151–186.

Lynn-Charney, C. & Rosen, D. (2000). Usage of accuracy models in stereolithography process planning. *Rapid Prototyping Journal*, *6*, 77–87.

Martin, I., del Castillo, D. S., Fernandez, A., & Güemes, A. (2020). Advanced thermoplastic composite manufacturing by in-situ consolidation: A review. *Journal of Physics D: Applied Physics*, *20*, 245–256.

Meiners, W., Wissenbach, K., & Gasser, A. (US Patent No. DE19649865 C1, 1998). Shaped body especially prototype or replacement part production.

Molitor, P., Barron, V., & Young, T. (2001). Surface treatment of titanium for adhesive bonding to polymer composites: a review. *International Journal of Adhesion & Adhesives*, *21*(2), 129–136.

Moroni, F., Pirondi, A., & Kleiner, F. (2010). Experimental analysis and comparison of the strength of simple and hybrid structural joints. *International Journal of Adhesion and Adhesives*, *30*(5), 367–379. Special Issue on Joint Design.

Parkes, P., Butler, R., Meyer, J., & de Oliveira, A. (2014). Static strength of metal-composite joints with penetrative reinforcement. *Composite Structures*, *118*, 250–256.

Perrin, H., Senoussaoui, N.-L., Dubief, C., & Vaudemont, R. (2021). Experimental investigation and optimization of thermal gradients by infrared welding. *ESAFORM 2021.*

Pocius, A. V. (1986). Fundamentals of structural adhesive bonding. In Hartshorn, S. R. (Ed.), *Structural Adhesives: Chemistry and Technology*, (pp. 23–68)., Boston, MA. Springer US.

Rafi, H., Nadimpalli, K., Gong, H., Starr, T., & Stucker, B. (2013). Microstructures and mechanical properties of ti6al4v parts fabricated by selective laser melting and electron beam melting. *Journal of Materials Engineering and Performance*, *22*, 248–.

Redmann, A., Damodaran, V., Tischer, F., Prabhakar, P., & Osswald, T. A. (2021). Evaluation of single-lap and block shear test methods in adhesively bonded composite joints. *Journal of Composites Science*, *5*(1).

Rennie, A. R. (1999). Thermoplastics and thermosets. In Swallowe, G. M. (Ed.), *Mechanical Properties and Testing of Polymers: An A–Z Reference*, (pp. 248–248)., Dordrecht. Springer Netherlands.

Sabancı University Integrated Manufacturing Center (2021). Unconventional and robotic manufacturing cell. https://suimc.sabanciuniv.edu/facilities/unconventional-and-robotic-manufacturing-cell.

Sercer, M. & Raos, P. (2010). Joining of plastics and composites. In Palmar, R. S. (Ed.), *Welding Engineering and Technology*. Khanna Publishers.

The Welding Institute (2004). A method of modifying surface structure by use of laser beams. International Patent WO 2004/028731 A1.

Tu, W., Guild, F., & Hogg, P. (2009). Comeld^{TM} joints: A novel technique for bonding composites and metal. *Rare Metal Materials and Engineering*, *38*, 134–141.

Ucsnik, S., Scheerer, M., Zaremba, S., & Pahr, D. (2010). Experimental investigation of a novel hybrid metal–composite joining technology. *Composites Part A: Applied Science and Manufacturing*, *41*(3), 369–374.

Wagner, G., Balle, F., & Eifler, D. (2013). Ultrasonic welding of aluminum alloys to fiber reinforced polymers. *Advanced Engineering Materials*, *15*(9), 792–803.

Wang, H., Xiao, X., Xiao, G., Fan, H.-T., & Arinez, J. (2019). Laser joining of carbon-fiber-reinforced polymer and metal with high-strength and corrosion-resistant bonds. *47th SME North American Manufacturing Research Conference, Pennsylvania*.

Wong, K. V. & Hernandez, A. (2012). A review of additive manufacturing. *ISRN Mechanical Engineering*, *2012*.

Zhang, D., Niu, W., Cao, X., & Liu, Z. (2015). Effect of standard heat treatment on the microstructure and mechanical properties of selective laser melting manufactured inconel 718 superalloy. *Materials Science & Engineering A*, *644*, 32–40.

Zhang, X., Duan, Y., Zhao, X., & Li, D. (2015). Uv stepwise cured fabrication of glass fiber/acrylate composites: Effects of exposure dose on curing uniformity and interlaminar shear strength. *Journal of Composite Materials*, *50*.

APPENDIX A

MATLAB code to calculate composite stiffness matrix for a laminate

```
clearvars
clc
%% Data Input
f_f=0.6;                          %fiber volume fraction
f_m=1-f_f;                        %matrix fraction

E_f=228*10^9 ;   v_f=0.22;   %fiber material properties (Pa)
E_m=3.5*10^9  ;   v_m=0.38;    %matrix material prperties (Pa)

%Lam=[0];
Lam=[0 0 0 0 0 0 0 0 0 0 0 0 0 0 0 0 0 0];  %Lamina angles [deg] ...
    from bottom to up. Add as many as you like in any orientation
t=0.127;                        %Lamina thickness (in mm, must be ...
    uniform)
%% Calculations
G_f=E_f/(2*(1+v_f));              %Shear modulus for fiber
G_m=E_m/(2*(1+v_m));              %Shear modulus for matrix

E11=f_f*E_f+f_m*E_m;              %Longitudinal elastic modulus
E22=((f_f/E_f)+(f_m/E_m))^-1;     %Lateral elastic modulus
v12=f_f*v_f+f_m*v_m;              %Poisson's ratio
G12=((f_f/G_f)+(f_m/G_m))^-1;     %Shear modulus

C=[ 1/E11        -v12/E11   0;    %Compliance matrix
    -v12/E11     1/E22      0;
    0                0    1/G12];

Q=inv(C);             % Reduced elastic stiffness of the lamina
N=numel(Lam);         % #of lamina layers as provided in the inputs
z=-t*N/2:t:t*N/2;     % Determining layer boundaries

S= [1 0 0;            % To transform lamina stiffness
    0 1 0;            % in eqn: T_tot=S*T*S^-1
    0 0 2];
A=zeros(3,3); B=zeros(3,3); D=zeros(3,3); %Preparing stiffness ...
    matrices
```

```
34
35 for i=1:N
36
37     %Transformation of lamina stiffness for every angle given in ...
           inputs.
38     %3x3xN sized data for N layers of lamina
39     T(:,:,i) = [cosd(Lam(i))^2                    sind(Lam(i))^2 ...
                           2*cosd(Lam(i))*sind(Lam(i));
40                  sind(Lam(i))^2                    cosd(Lam(i))^2 ...
                                       -2*cosd(Lam(i))*sind(Lam(i));
41                 -sind(Lam(i))*cosd(Lam(i))        ...
                      sind(Lam(i))*cosd(Lam(i))        ...
                      cosd(Lam(i))^2-sind(Lam(i))^2];
42
43     Ttot(:,:,i)  = S * T(:,:,i) * inv(S);            %magic
44     Q_bar(:,:,i) = inv(T(:,:,i)) * Q * Ttot(:,:,i); %transformed ...
           stiffness matrices
45
46     A=A+Q_bar(:,:,i)*(z(i+1)   -z(i))    ;          % Stiffness ...
           matrices for the combined laminate
47     B=B+Q_bar(:,:,i)*(z(i+1)^2 -z(i)^2)/2;
48     D=D+Q_bar(:,:,i)*(z(i+1)^3 -z(i)^3)/3;
49
50 end
51
52 %% Applying strain to find forces and moments created
53 e=[1;0;0;0;0;0];
54 K=[0;0;0;0;0;0];
55 CSM=[A B;B D];
56 PM=[A B;B D]*[e K];
57 P=PM(:,1); M=PM(:,2);
58
59 % B values are 1e-12 times a matrix. It's practically zero.
60 % since [P;M] = [A B; B D]*[e;K] and thus P=Ae+BK, it's proven that
61 % normal forces won't cause bending or twisting. This is ...
       expected from
62 % the symmetric and balanced laminate we've created.
63 end
```